ACS OMEGA

Open Access

http://pubs.acs.org/journal/acsodf

Article

Fe_3O_4–Chitosan Nanocomposite as a pH-Responsive Delivery System for Enhanced Delivery of *Punica Granatum* L. Polyphenols

Ravimal Rukshan, Nisal Rajapaksha, Supuni Wijayawardana, Charitha Thambiliyagodage,* Udani Senevirathne, Madara Jayanetti, and Upeka Samarakoon

Cite This: *ACS Omega* 2025, 10, 50488–50510

Read Online

ACCESS | Metrics & More | Article Recommendations | Supporting Information

ABSTRACT: *Punica granatum* extract (PG), consisting of punicalagin, ellagic acid, and gallic acid, was loaded onto an Fe_3O_4/Chitosan (Fe_3O_4@Chi) nanocomposite (Fe_3O_4@Chi-PG) to enhance pharmacokinetic properties. Fe_3O_4 was synthesized via the coprecipitation method and coupled with chitosan in 2% acetic acid solution via glutaraldehyde cross-linking. The presence of interested polyphenols in the pomegranate extract was confirmed by HPLC analysis, and the extract was post-loaded to the nanocarrier. XRD confirmed the crystallographic orientation of the nanocarrier, and SEM analysis confirmed the successful coupling of Fe_3O_4 onto the chitosan surface during the fabrication of Fe_3O_4@Chi. BET surface area analysis revealed the presence of micro- and mesopores in the synthesized materials. Significant reduction of the BET surface area and the pore volume of Fe_3O_4@Chi-PG compared to Fe_3O_4@Chi suggested the loading of the porous network and surface by PG. The presence of vibrational bands corresponding to the functional groups of the relevant bioactive compounds was confirmed via FT-IR analysis. The IC_{50} values of the nanocomposite for DPPH and egg albumin denaturation assays were 18.69 and 257.69 μg/mL, respectively. The PG encapsulation efficiency of Fe_3O_4@Chi-PG was reported to be 86.44%. The pH-responsive release of the polyphenols was studied by fitting the release data into five kinetic models, including Korsemeyer–Peppas (KP) and Peppas–Sahlin (PS). The KP and PS models were selected to interpret the release mechanism based on the $R^2 \geq 0.95$ value. A combination of Fickian diffusion, relaxation, and swelling dominates the polyphenol release. Quasi-Fickian diffusion is responsible for the release in media with pH 1–6.7, whereas anomalous transport occurs at pH 7.4 ($n = 0.46$) according to the KP model. Polymer relaxation is the dominant mechanism for the release of bioactive compounds at pH 7.4, as exhibited by R/F > 1. However, the contribution of relaxation to the release of polyphenols at pH 2.5, 4, and 5.5 was negligible according to the parameters ($k_R = 0$). Characteristics of chitosan, including protonation and deprotonation of NH_2 groups, surface charge of Fe_3O_4, ionization of COOH and OH groups of the polyphenols, and molecular weight of the active compounds, contributed to the differences in the release behavior.

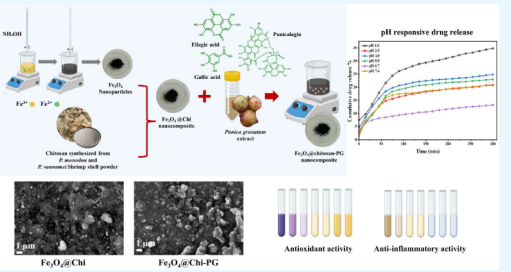

1. INTRODUCTION

Pomegranate (*Punica granatum* L.) is a deciduous small tree that belongs to the family Punicaceae and is cultivated in tropical and subtropical regions worldwide.[1] Apart from its nutritional value, pomegranate is well-known for its medicinal properties.[2,3] Studies indicate that different components of pomegranate fruit contain biologically active compounds with anticancer,[4−6] antioxidant,[7−9] anti-inflammatory,[10,11] antidiabetic,[12,13] antibacterial[14,15] and hypolipidemic activities.[16] Punic acid is the major fatty acid present in pomegranate seed oil, and in addition to that, anthocyanins, phenolic acids, flavonoids, and coumarins are present in pomegranate seeds.[17] Pomegranate peel is a source of secondary metabolites, including flavonoids and hydrolyzable tannins (punicalagin, punicalin, ellagic acid, and gallic acid). Punicalagin is the most abundant ellagitannin type found in the pomegranate peel, which can be hydrolyzed into ellagic acid upon exposure to strong acids or microorganisms.[1,18] Punicalagins are well-known for their strong ability to scavenge free radicals, including hydroxyl, superoxide anion, and singlet oxygen radicals, as well as their ability to suppress lipid peroxidation.[19]

The Biopharmaceutics Classification System (BCS) is a scientific framework that uses intestinal permeability and aqueous solubility to classify medicinal compounds.[20] Polyphenols should undergo pharmacological metabolic processes that will result in their conversion into more soluble metabolites and their subsequent excretion in order to exhibit their therapeutic impact. In mammals, these compounds are subjected to phase I and phase II metabolism, where ingested O-glycoside conjugates are converted to corresponding aglycones via a hydroxylation reaction, followed by liver-

Received: August 9, 2025
Revised: October 9, 2025
Accepted: October 13, 2025
Published: October 17, 2025

conjugated metabolism to become O-glucuronides and O-sulfates.[21] The lower bioavailability and faster excretion are caused by the rapid metabolism of gallic acid under the above-mentioned pathways.[22] It is classified as class III medication in BCS, with high solubility and low permeability.[23] Higher molecular weight, which restricts absorption by simple diffusion, and extremely low lipid solubility, which limits permeability across the gastrointestinal tract's (GIT) bilipid layer, are two of the reasons given for the poor bioavailability of punicalagin.[24,25] Furthermore, the intestinal microbiota of healthy people converts punicalagins into hydroxy-6H-dibenzopyran-6-one derivatives (urolithins), which are bioavailable but not very effective antioxidants.[19] Poor bioavailability of ellagic acid (EA) is associated with its low solubility, limited permeability, fast metabolism, and removal from the system. Both punicalagin and EA are categorized as class IV medications by the BCS.[26] Only a small portion of EA derived from ellagitannis is absorbed in the stomach owing to its resistance to acidic pH. Colon microflora convert ellagitannins and EA to urolithins, facilitating cellular uptake. However, owing to the variability of the gut microbiota composition, each individual may produce highly or less active urolithins or no urolithins, resulting in varied health benefits across the population.[27] Thus, drug delivery systems such as nanoparticles,[28,29] nanoemulsions,[30,31] solid-lipid nanoparticles,[32] hydrogels,[33] and polymeric nanoparticles[34,35] have been used to overcome these drawbacks related to lower bioavailability and rapid metabolism of the above-mentioned polyphenols.

Iron oxide nanoparticles (Fe_3O_4 NPs) are one of the many types of NPs that have gained attention because of their remarkable superparamagnetic properties, biocompatibility, extremely low toxicity, biodegradability, and reactive surface amenable to modification using biocompatible coatings. Fe_3O_4 NPs are used extensively in drug delivery systems owing to their superparamagnetic properties and easily modifiable particle surfaces. Drug delivery systems consisting of Fe_3O_4 NPs can be directed to the target site using external magnetic fields.[36] As a result, research has been conducted on manipulating superparamagnetic Fe_3O_4 NPs using external magnetic fields in order to deliver a variety of medicinal chemicals precisely.[37,38] Recent research has considered functionalizing Fe_3O_4 NPs with a variety of materials, including silica,[39] carbon,[40] graphene oxide,[41] and polymers.[42] Thus, polymers with magnetic sensitivity resulting from the incorporation of Fe_3O_4 NPs with polymers will pave the way to address the conventional limitations in remotely controlled targeted drug administration.

A cationic polymer, chitosan, is produced by partially deacetylating chitin, a copolymer made up of 2-amino-2-deoxy-D-glucose and 2-acetamido-2-deoxy-D-glucose units with β-(1−4) links.[38] Chitosan is being used in biomedical applications owing to its nontoxic, mucoadhesive, biocompatible, and biodegradable properties.[43] It has been used for the delivery of therapeutic agents, including anticancer drug doxorubicin (DOX),[44,45] nonsteroidal anti-inflammatory drug indomethacin,[46] curcumin targeting the treatment of inflammatory bowel disease,[47] and ciprofloxacin.[48] At physiological pH, chitosan is a weak base with a positive charge (pK_a value ∼ 6.5).[49] The amine and hydroxyl groups of the chitosan chains facilitate interactions with other materials, including Fe_3O_4 NPs, in synthesizing nanocomposites.[42] In addition to having reduced toxicity and improved biocompatibility, functionalized Fe_3O_4 NPs with chitosan will interact with biological molecules such as DNA, polypeptides, and antibodies.[50] Accordingly, chitosan was used as the material to couple with Fe_3O_4 NPs in the current study to enhance the biological activity of the designed delivery system.

Natural therapeutic compounds, including curcumin[51,52] and pomegranate peel extract,[34] and synthetic therapeutic compounds, including doxorubicin,[53] indomethacin,[46] and hydrocortisone,[54] have been incorporated into delivery systems consisting of chitosan and Fe_3O_4 in various studies. In the present study, a chitosan-loaded Fe_3O_4 NP delivery system (Fe_3O_4@Chi) was used to deliver the polyphenolic compounds of the *Punica granatum* seed/peel extract. The presence of punicalagin, EA, and gallic acid was confirmed via HPLC analysis, and the *in vitro* drug release kinetics were evaluated using five kinetic models under varying pH media compositions. Furthermore, the antioxidant and anti-inflammatory potential was assessed. Several attempts have been made to deliver pomegranate extract and the respective polyphenolic compounds using chitosan, Fe_3O_4 and a combination of these with other polymer delivery systems.[55−58] Even though pomegranate extract has been used as a reducing and stabilizing agent to synthesize Fe_3O_4 NPs extensively,[59−63] to our knowledge, research focused on the delivery of punicalagin, EA, and gallic acid derived from the pomegranate peel/seed extract (PG) using Fe_3O_4@Chi nanocomposite delivery systems has not been conducted. Moreover, a detailed release kinetics analysis over a varied pH range has not been reported in the literature for the delivery of polyphenolic compounds of PG using an Fe_3O_4@Chi delivery system. Therefore, the present study focused on evaluating the pH-responsive delivery of punicalagin, EA, and gallic acid of pomegranate extract using the Fe_3O_4@Chi nanocomposite. The study provides valuable insight into the pH-responsive delivery of the respective bioactive compounds, filling critical research gaps in polyphenol delivery systems.

2. METHODOLOGY

2.1. Extraction of Bioactive Compounds from Pomegranate. Fresh pomegranate fruits of the local "Nimali" cultivar were initially washed thoroughly using distilled water to remove any impurities. The fruits were then manually separated into peels and seeds. Both the peels and seeds were dried in a hot air oven at 40 °C until they reached a constant weight. The dried materials were ground into a fine powder. Equal proportions (1:1 w/w) of peel powder and seed powder were mixed and extracted by using methanol in a 1:5 (w/v) sample-to-solvent ratio. The mixture was shaken continuously for 24 h and subjected to ultrasonication for 1.5 h at room temperature (25 °C) to enhance extraction efficiency. The suspension was centrifuged to collect the supernatant, while the pellet was re-extracted under the same conditions. Both supernatants were pooled and evaporated to obtain the crude bioactive extract.[64] The extraction yield was calculated to be 41.62% (w/w). The resulting crude extract was stored in a sealed amber glass vial at −20 °C until use.

2.2. Synthesis of Fe_3O_4 Nanoparticles via Coprecipitation. The Fe_3O_4 NPs were synthesized using a coprecipitation method. In this process, ferric chloride ($FeCl_3$) and ferrous sulfate heptahydrate ($FeSO_4{\cdot}7H_2O$) in a 2:1 molar ratio were dissolved in 200 mL of distilled water under continuous stirring (400 rpm). To facilitate the precipitation of magnetite, 25% ammonium hydroxide (NH_4OH) was added dropwise to reach pH 11.0, while maintaining the temperature

https://doi.org/10.1021/acsomega.5c08001
ACS Omega 2025, 10, 50488−50510

60 ± 5 °C. Fe_3O_4 was precipitated, which was washed several times with distilled water to neutralize the pH, and dried at 60 °C in a hot air oven.[65] The sample was stored in an airtight container at room temperature for further use.

2.3. Preparation of Chitosan from Shrimp Shells. Shrimp shells were collected and cleaned using 70% isopropyl alcohol to remove impurities. After oven drying (80 °C), the shells were ground into a coarse powder. Demineralization was conducted by immersing the powdered shells in 10% hydrochloric acid (HCl) for 24 h at room temperature (25 °C). After the powder was washed to neutralize the pH, the residue was stirred in 3% sodium hydroxide (NaOH) media for 5 h at 25 °C, allowing deproteinization. Deacetylation was followed by refluxing the powder in 50% NaOH for 2 h at 80 °C, where chitin from the shells was converted to chitosan. The resulting powder was dried by using a hot air oven (60 °C). The sample was stored in an airtight container at room temperature for further use and analysis.[66]

2.4. Synthesis of Chitosan−Fe_3O_4 Nanocomposite. A chitosan solution was prepared by dissolving 5 g of chitosan in 500 mL of 2% acetic acid, followed by magnetic stirring at 500 rpm for 12 h to ensure complete solubilization. Subsequently, 5 g of Fe_3O_4 NPs were gradually added to the chitosan solution, and the mixture was stirred continuously for 3 h. To functionalize chitosan and Fe_3O_4 NPs and to stabilize the composite, glutaraldehyde (50 wt %, 1 mL) was introduced as the cross-linking agent and stirred for 3 h. Thereafter, 1 M NaOH was slowly added dropwise until the solution reached a neutral pH of 7. The final mixture was left undisturbed overnight to facilitate complete precipitation. All of the steps of the experiment were carried out at room temperature (25 °C). The resulting precipitate was filtered, washed with distilled water, and dried at 40 °C.[42] The sample was stored in an airtight container at room temperature for further use.

2.5. Loading of Fe_3O_4−Chitosan Nanocomposite with Pomegranate Extract. To load the synthesized nanocomposite with pomegranate bioactive compounds, 3 g of the crude extract was dissolved in 100 mL of methanol. An equal amount (3 g) of the Fe_3O_4−chitosan nanocomposite was added to this solution, and the mixture was stirred at 300 rpm overnight at room temperature (25 °C) to ensure adsorption and loading of the extract onto the composite surface. Following solvent evaporation, the final loaded nanocomposite was dried at 40 °C and stored in an airtight container at −20 °C until further use.

2.6. Characterization. X-ray diffraction (XRD) patterns were acquired by using a D8 Advance Bruker diffractometer equipped with Cu Kα radiation (λ = 0.154 nm). The diffraction angle (2θ) was scanned from 5° to 80° at a rate of 2°/min. The surface morphology of the synthesized materials was examined using a ZEISS EVO 18 RESEARCH scanning electron microscope (SEM). Vibrational fingerprints of the synthesized material were acquired in the mid-infrared region (4000−500 cm^{-1}) using a Vertex 70-RAM II Bruker spectrometer equipped with a diamond attenuated total reflectance (ATR) accessory at a resolution level of 4 cm^{-1}, averaging 256 scans per spectrum. Surface area and pore size distribution were evaluated by a Quantachrome V2.0 instrument. The samples were degassed at 200 °C for 12 h to collect the adsorption−desorption isotherms.

2.7. HPLC Analysis. The *Punica granatum* L. methanolic extract was filtered through a 0.45 μm nylon syringe and directly injected for analysis. The HPLC fingerprint of the methanolic *P. granatum* L. extract was obtained using an Agilent 1200 HPLC system equipped with a ZORBAX Eclipse XDB-C18 column (4.6 mm × 150 mm, 5 micron). Detection was carried out at 254 nm using a UV−vis detector. The mobile phase consisted of (A) acetonitrile (HPLC grade) and (B) 0.5% (v/v) acetic acid in distilled water delivered at a flow rate of 1.0 mL/min. Gradient elution was employed as follows: initially 0% A (100% B), linearly increased to 30% (A) at 40 min, 60% (A) at 60 min, and 90% (A) at 62 min, held until 68 min, followed by re-equilibration to initial conditions by 70 min. The total running time was 70 min, and the column temperature was maintained at 30 °C. The injection volume was 20.0 μL.[67]

2.8. Antioxidant Activity Using DPPH Assay. The antioxidant capacity of the nanocomposite was evaluated by using the DPPH radical scavenging method. A 1 mM stock solution of DPPH in methanol was prepared. Test solutions were prepared by diluting the extract and loaded nanocomposite in methanol to obtain concentrations ranging from 5 to 35 μg/mL. Each dilution (5 mL) was mixed with 0.5 mL of the DPPH solution and incubated in the dark for 30 min. Absorbance at 517 nm was measured by using a UV−vis spectrophotometer. The radical scavenging activity (RSA%) was calculated using the following formula:

$$\mathrm{RSA\%} = \left(\frac{A_{\mathrm{control}} - A_{\mathrm{sample}}}{A_{\mathrm{control}}}\right) \times 100\% \quad (1)$$

where $A_{control}$ is the absorbance of the DPPH solution without the sample and A_{sample} is the absorbance in the presence of the tested compounds. Each experiment was triplicated, and the results were reported as mean ± standard error. The concentration to result in 50% inhibition (IC_{50}) was determined using the nonlinear curve fitting method (OriginLab) by plotting the RSA% over the concentration of the sample.[68,69]

2.9. Egg Albumin Denaturation Assay. The anti-inflammatory activity of the nanocomposite and pomegranate extract was evaluated by using the protein denaturation method. The concentration of the test compounds varied from 50 to 250 μg/mL. To each tube with 2 mL of the test sample in methanol, 2.8 mL of phosphate-buffered saline (PBS, pH 6.4) and 0.2 mL of 1% egg albumin solution were added to maintain the desired reaction conditions. The samples were incubated at 37 °C for 30 min to enable interaction with inflammatory mediators, followed by heating in a water bath at 70 °C for 15 min to induce protein denaturation. After cooling to ambient temperature, absorbance was recorded at 600 nm and 800 nm using a UV−vis spectrophotometer. The absorbance difference (ΔA) was calculated as follows:

$$\Delta A = A_{600\,\mathrm{nm}} - A_{800\,\mathrm{nm}} \quad (2)$$

This differential absorbance was used to compute the percentage inhibition using the following formula:

$$\text{Percentage inhibition} = \left(\frac{A_{\mathrm{control}} - A_{\mathrm{sample}}}{A_{\mathrm{control}}}\right) \times 100\% \quad (3)$$

where $A_{control}$ represents ΔA of the control (without sample) and A_{sample} represents ΔA of the test sample. Mean RSA values were obtained for each concentration, and the corresponding percentage inhibition of protein denaturation was plotted to evaluate the dose-dependent anti-inflammatory efficacy of the

https://doi.org/10.1021/acsomega.5c08001
ACS Omega 2025, 10, 50488−50510

formulations. The IC_{50} value was determined by the linear regression model.[68]

2.10. Drug Encapsulation Efficiency % and Loading Degree %. EE% of Fe_3O_4@Chi-PG was determined with slight modifications.[70] Freshly prepared Fe_3O_4@Chi-PG was dissolved in methanol and sonicated at room temperature for 15 min. Afterward, 5 mL of the suspension was extracted and subjected to centrifugation at 6000 rpm for 30 min. The supernatant with the unbound drug was then collected, and the absorbance for unloaded bioactive compounds was measured at 360 nm using UV−visible spectroscopy.[71] Utilizing the PG extract as a standard solution, a calibration curve was plotted. In brief, the amount of the unloaded drug in parts per million was determined by utilizing the calibration curve to convert the supernatant absorption to the drug concentration. The amount of free drug was obtained by multiplying the drug concentration by the volume of the drug utilized in the drug-loading procedure.[72,73] The encapsulation efficiency (EE %) was calculated using the following formula:

$$\mathrm{EE}(\%) = [\text{Amount of loaded drug(mg)}] / [\text{Total amount of drug(mg)}] \times 100 \quad (4)$$

Loading degree (LD%) was calculated using the following formula:

$$\mathrm{LD}(\%) = [\text{Amount of loaded drug(mg)} / \text{Total weight of drug + system(mg)}] \times 100 \quad (5)$$

where the substitution between the initial amount of the drug and free drug will result in the amount of the loaded drug.

2.11. In Vitro Drug Release Study. The release profile of the pomegranate-loaded nanocomposite was assessed in media of varying pH values (1.0, 2.5, 4.0, 5.5, 6.7, and 7.4). An amount of 2.5 mg of the nanocomposite was dispersed in closed cuvettes containing the release medium and incubated at room temperature (25 °C). Absorbance was measured every 15 min over a period of 5 h at 360 nm[71] using a UV−vis spectrophotometer to determine the cumulative amount of released bioactive compounds.[68]

The cumulative drug release (CDR)% for every media composition was calculated using the following equation:

$$\%\,\mathrm{CDR} = \frac{\text{Amount released at time}(t)}{\text{Total amount of drug loaded into DDS}} \times 100\% \quad (6)$$

The drug release data were analyzed using mathematical models to understand the underlying release mechanisms, and the best-fit models with $R^2 \geq 0.95$ were selected to evaluate the release mechanism of the polyphenolic compounds from the delivery system.

The following equation shows the zero-order kinetics model:

$$Q_t = Q_0 + k_0 t \quad (7)$$

Q_t represents the amount of active agent released during time t and k_0 is the zero-order constant.

The first-order kinetic model is expressed as follows:

$$Q_t = Q_0(1 - e^{-k_1 t}) \quad (8)$$

Q_t is the amount of active agents released at time t, Q_0 is the initial amount of the drug dissolved, and k_1 is the first-order constant.

The following equation indicates the Higuchi kinetic model:

$$Q_t = k_H t^{1/2} \quad (9)$$

Q_t is the amount of drug released at time t and k_H is the Higuchi constant.

The Korsmeyer−Peppas model is denoted by the following equation:

$$Q_t = k_P t^n \quad (10)$$

Q_t is the amount of drug released over time t, where n is the exponent of release (related to the drug release mechanism) as a function of time t, and k_P is the model constant.

The Peppas−Sahlin model is expressed in eq 11, which determines the estimated diffusional and relaxational contributing mechanisms in an anomalous drug release process.

$$Q_t = (k_D t^m) + (k_R t^{2m}) \quad (11)$$

Here, the constants k_D, k_R, and m are implemented. The first part of the equation represents the Fickian diffusional contribution (F), whereas the second term (Case II) represents the relaxational contribution (R). The coefficient m represents the strictly Fickian diffusion exponent for each system with regulated release.

The following formula can be used to determine the ratio of the R and F contributions:

$$\mathrm{R/F} = k_R t^m / k_D \quad (12)$$

3. RESULTS AND DISCUSSION

3.1. XRD Analysis. The XRD patterns of the synthesized materials were collected to determine crystallography (Figure 1). The XRD pattern of chitosan shows characteristic peaks at 19.3°, 20.9°, 22.9°, and 26.4° corresponding to the (110), (120), (101), and (130) crystalline planes (JCPDS card number 39-1894), with d spacings of 0.46, 0.42, 0.39, and 0.34 nm, respectively. The calculated crystallite size is 5.05 nm. The XRD pattern of Fe_3O_4 shows the characteristic peaks of magnetite at 30.2°, 35.6°, 43.2°, 53.6°, 57.2°, and 62.8°, which are attributed to (220), (311), (400), (422), (511), and (440) (JCPDS card no: 19-0629), and the corresponding d spacing values are 0.30, 0.25, 0.21, 0.17, 0.16, and 0.15 nm, respectively. The calculated crystallite size is 10.63 nm. Both XRD patterns of Fe_3O_4@Chi and Fe_3O_4@Chi-PG show the characteristic peaks of chitosan and Fe_3O_4. The absence of any new crystalline peaks in Fe_3O_4@Chi-PG suggests that PG did not disrupt the crystallinity of the nanocomposite. There is no change in the crystallite size or the d spacing when materials are coupled together and loaded with PG. All of the parameters related to the crystallography of the materials are tabulated in Table 1. According to the results, no significant changes were observed in the crystallite size or the d spacing when materials are coupled (Fe_3O_4@Chi and Fe_3O_4@Chi-PG). As the processes of coupling chitosan and loading with PG occur after the synthesis of Fe_3O_4 NPs and chitosan, subsequently, the crystal lattice of Fe_3O_4 NPs is not disturbed. Therefore, they do not alter the internal atomic arrangement or the size of the formed crystallites.

3.2. SEM. SEM images were collected to study the surface morphologies of the synthesized materials. The SEM image of chitosan (Figure 2a) shows an oval-shaped macropore structure, which was established due to the removal of minerals ($CaCO_3$) and protein upon treatment with 10%

https://doi.org/10.1021/acsomega.5c08001
ACS Omega 2025, 10, 50488−50510

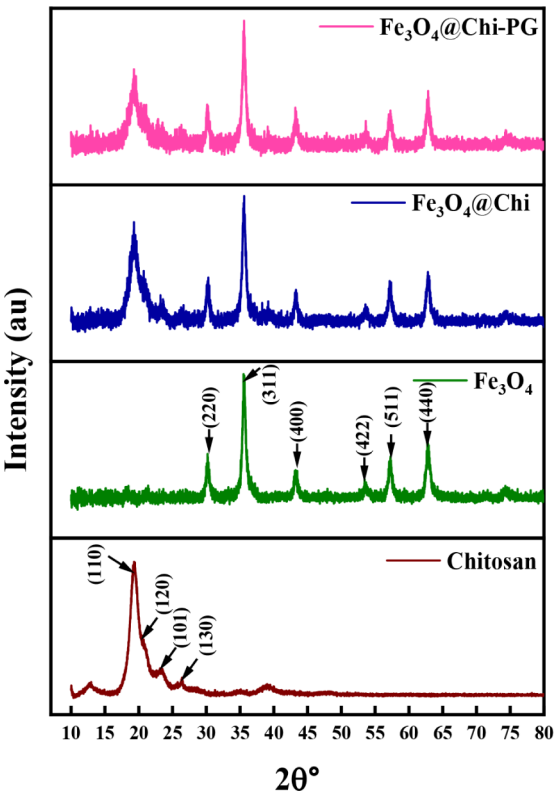

Figure 1. XRD pattern of the synthesized materials.

Table 1. Crystallographic Parameters of the XRD Patterns

Sample	Crystal plane	2θ°	L (nm)	d (nm)	L/d
Chitosan	110	19.34	5.05	0.46	10.98
Fe_3O_4	311	35.61	10.63	0.25	42.52
Fe_3O_4@Chi	110	19.31	4.52	0.46	9.83
	311	35.59	13.62	0.25	54.48
Fe_3O_4@Chi-PG	110	19.28	4.45	0.46	9.67
	311	35.60	10.78	0.25	43.12

HCl and 3% NaOH in the conversion of chitin to chitosan. The SEM image of Fe_3O_4 nanoparticles (Figure 2 b) shows nanoparticles with a diameter of 62.48 ± 0.76 nm (Figure 2c) and spherical and irregularly shaped aggregates with a diameter of 170.85 ± 1.92 nm (Figure 2d). As exhibited in the SEM image of the chitosan−Fe_3O_4 nanocomposite (Figure 2e), the well-established oval-shaped macropores of the chitosan matrix, which were formed after the removal of proteins during the deproteination step of chitosan synthesis, can no longer be seen in the SEM image of Fe_3O_4@Chi. Fe_3O_4 NPs are heterogeneously distributed on the chitosan matrix, where the density of the nanoparticles varies from one location to another. A new macropore structure with irregularly shaped macropores of different sizes has been formed after the coupling of Fe_3O_4. The chitosan−Fe_3O_4 nanocomposite consisted of particles with an average size of 93.01 ± 2.04 nm (Figure 2 f) and aggregates of the same with a diameter of 176.42 ± 5.00 nm (Figure 2g). Aggregates of both Fe_3O_4 nanoparticles and chitosan−Fe_3O_4 nanocomposites were formed during synthesis and aging to neutralize the surface charge. Furthermore, they physically interact with each other, forming clumps and aggregates for a thermodynamically favorable arrangement. During the formation of chitosan−Fe_3O_4 nanocomposites, hydroxyl groups on the surface of Fe_3O_4 interact with the NH_2 groups of chitosan to form a complex. Fe_3O_4 can interact with the NH_2 groups of different chitosan molecules. During the formation of such linkages, aggregates can be formed. Furthermore, glutaraldehyde was used as a cross-linker to link chitosan molecules that had already formed a complex with Fe_3O_4, thereby establishing a network of chitosan−Fe_3O_4. This can lead to the production of aggregates of chitosan−Fe_3O_4 nanocomposites. Pomegranate extract has masked the chitosan−Fe_3O_4 nanocomposite during the deposition of the extract on the surface of the nanocomposite, as illustrated in the SEM image of chitosan−Fe_3O_4 nanocomposite-pomegranate (Figure 2h).

3.3. BET Analysis. The surface area and pore size distributions of the synthesized materials were determined. The adsorption−desorption isotherms (Figure 3a) exhibited type V isotherms with H3 hysteresis loops, indicating the presence of poorly developed micropores, as suggested by the slow increase in adsorption at relatively low pressures. Thereafter, adsorption increases significantly, demonstrating a huge number of mesopores on the adsorption platform. The surface area and pore volume of chitosan are comparatively lower, indicating the presence of a low amount of mesopores and micropores, though the material is abundant in larger macropores, as shown in the SEM image in Figure 2a. The bulky molecules, including proteins, were removed during the synthesis of chitosan, hence facilitating the formation of macropores.[66] The high surface area, pore volume, and pore size resulting in Fe_3O_4 suggest the presence of an abundant amount of micropores and mesopores. The surface area and the total pore volume of Fe_3O_4@Chi have been reduced to 45.47 m^2/g and 0.162 cm^3/g, respectively, compared to those of Fe_3O_4, but are significantly higher than those of chitosan (Table 2). This resulted from the weight ratio in which chitosan and Fe_3O_4 were coupled (1:1), where Fe_3O_4 mainly contributed to the textural properties of the composite. The same parameters of Fe_3O_4@Chi-PG have been reduced to 3.12 m^2/g and 0.013 cm^3/g, suggesting the loading of PG in the porous network and on the surface of the delivery system. The average pore size increased from 7.134 to 7.428 nm, indicating the creation of larger mesopores after loading of PG. Pore size distribution data are represented in Figure 3b, indicating the presence of micro- and mesopores in the synthesized material.

3.4. FT-IR. The FT-IR spectra were obtained to study the different functional groups present in the materials and to confirm the loading of Fe_3O_4@Chi with PG. The peaks on the FT-IR spectrum of chitosan centered at 1008 and 1066 cm^{-1} correspond to the symmetric and asymmetric C−O−C stretching vibrations. The peak at 1307 cm^{-1} is assigned to C−H bending, and the peak at 1378 cm^{-1} is attributed to C−H bending of the alkane, while the peak at 1548 cm^{-1} represents N−H bending of the amine group. The peak at 1655 cm^{-1} corresponds to the C═O stretching, suggesting the presence of acetyl groups, which were not deacetylated upon treatment with 50% NaOH. The peaks at 2874 cm^{-1} and 3097 cm^{-1} are attributed to the C−H stretching, whereas the peak at 3248 cm^{-1} is assigned to the O−H stretching of the hydroxyl groups. The broad peak at 3447 cm^{-1} corresponds to the N−H stretching of the amine group. The increase in the absorbance in the region below 1000 cm^{-1} of Fe_3O_4 nanoparticles confirms the presence of Fe−O vibrations. The vibrational band near 572 cm^{-1} is attributed to the Fe−O stretching vibration. Coupling of Fe_3O_4 onto the surface of chitosan can be confirmed by the presence of characteristic vibration bands,

https://doi.org/10.1021/acsomega.5c08001
ACS Omega 2025, 10, 50488−50510

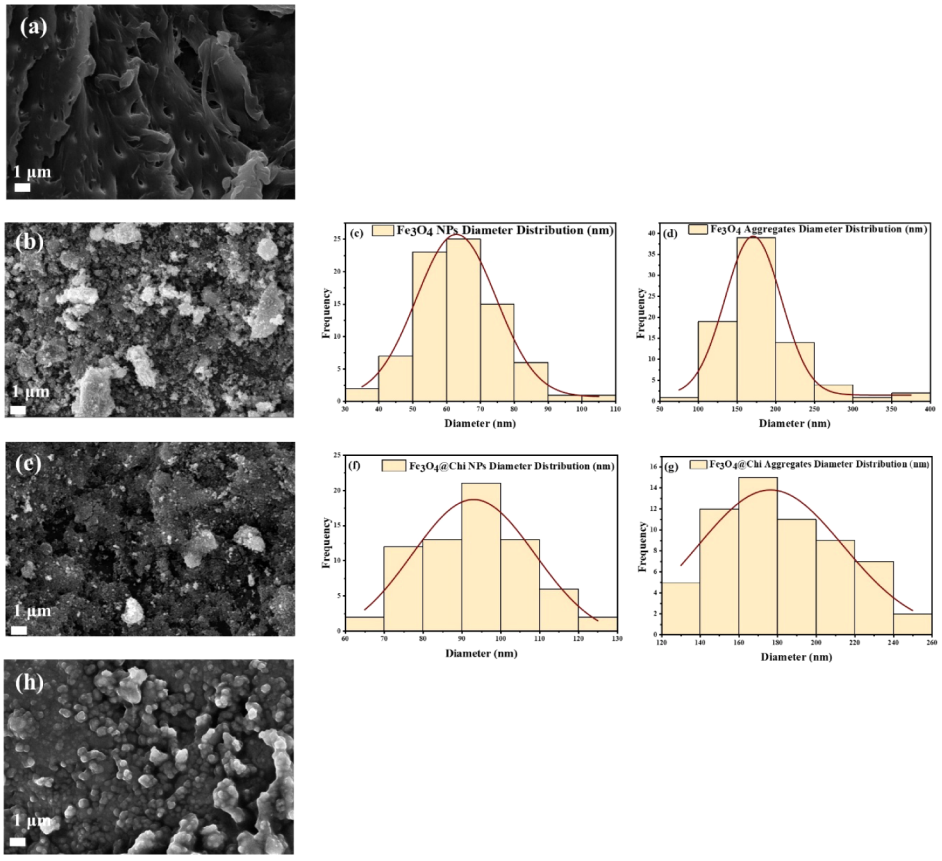

Figure 2. (a) SEM image of chitosan, (b) SEM image of Fe_3O_4 nanoparticles, (c) particle size distributions of Fe_3O_4 NPs, (d) particle size distributions of Fe_3O_4 aggregates in Fe_3O_4 NPs, (e) SEM image of the Fe_3O_4/chitosan composite (Fe_3O_4@Chi), (f) particle size distributions of Fe_3O_4 NPs in Fe_3O_4@Chi, (g) particle size distributions of Fe_3O_4 aggregates in Fe_3O_4@Chi, and (h) SEM image of Fe_3O_4@Chi-PG.

including 1007 cm^{-1}, 1070 cm^{-1}, 1623 cm^{-1}, and 1664 cm^{-1} in the FT-IR spectra of Fe_3O_4@Chi, as indicated in Figure 4. The same bonds of chitosan spectra were present in Fe_3O_4@Chi, though the peak positions vary slightly due to the coupling of chitosan with Fe_3O_4. The FT-IR spectrum of PG shows many characteristic peaks. The peaks below 920 cm^{-1} represent the C═C bending, and the broad, significant peak at 1032 cm^{-1} is attributed to the C−O stretching of the active compounds of PG. The peak at 1243 cm^{-1} is assigned to the C−O stretching in aromatic esters, present in punicalagin, which is one of the active compounds in PG, and the peak at 1347 cm^{-1} represents the O−H bending of the hydroxyl group of the active ingredients. The peak at 1446 cm^{-1} is assigned to C−H bending, while the peak at 1609 cm^{-1} corresponds to the C═C stretching frequency. The C═O stretching is represented by the peak at 1723 cm^{-1}, and the peaks at 3299 cm^{-1} represent the hydroxyl groups. The presence of the characteristic peaks of PG on Fe_3O_4@Chi with slight variations in peak positions suggests the successful loading of PG on Fe_3O_4@Chi. Table S1 indicates a detailed representation of the FT-IR vibrational bands and their corresponding functional groups. These data further confirm the coupling of Fe_3O_4 with chitosan and the loading of PG onto the surface of Fe_3O_4@Chi.

3.5. HPLC Analysis. The HPLC fingerprint of *P. granatum* methanolic extract was analyzed with ellagic acid, gallic acid, and punicalagin α, β commercial standards (Figure S1). The complete chromatogram is presented in Figure 5, and the respective details of the elution of the compounds are indicated in Table 3. The characteristic peaks that correspond to punicalagin α and β, ellagic acid, and gallic acid can be identified in the extract among other distinctive peaks, which could be attributed to other chemical compounds present in the extract. Furthermore, the UV spectra of the extract peaks were compared to the standards to verify the identification's specificity. Based on the experimental results and previously published literature,[74−77] all of these chemicals are inferred to be major polyphenolic compounds of the *P. granatum* extract.

3.6. Antioxidant Activity. The DPPH radical scavenging assay was used to evaluate the antioxidant activity of PG and the Fe_3O_4@Chi-PG composite. Both samples showed an increase in Radical Scavenging Activity (RSA%) with concentration, suggesting a dose-dependent antioxidant response. Figure 6a,b depicts the variation of RSA% vs concentration. The concentration ranges used to evaluate the RSA% ranged between 5−30 and 5−35 μg/mL for the pomegranate extract and for the nanocomposite, respectively. Concentrations above 30 μg/mL were not used to assess the RSA% of the pomegranate extract to eliminate saturation effects. IC_{50} values were calculated using nonlinear curve fitting of the collected data (n = 3). Ascorbic acid was used as the positive control.

The RSA% of the PG was reported to range between 25.20 ± 1.25% at 5 μg/mL concentration and reached a maximum value of 95.61 ± 0.06% at 30 μg/mL. In contrast, Fe_3O_4@Chi-PG exhibited a slightly lower RSA% varying between 12.78 ± 0.97% and 84.86 ± 0.45% at 5 and 35 μg/mL concentrations, respectively. It is worth noting that at lower concentrations (<20 μg/mL), PG's RSA% was nearly 2 times that of Fe_3O_4@

https://doi.org/10.1021/acsomega.5c08001
ACS Omega 2025, 10, 50488−50510

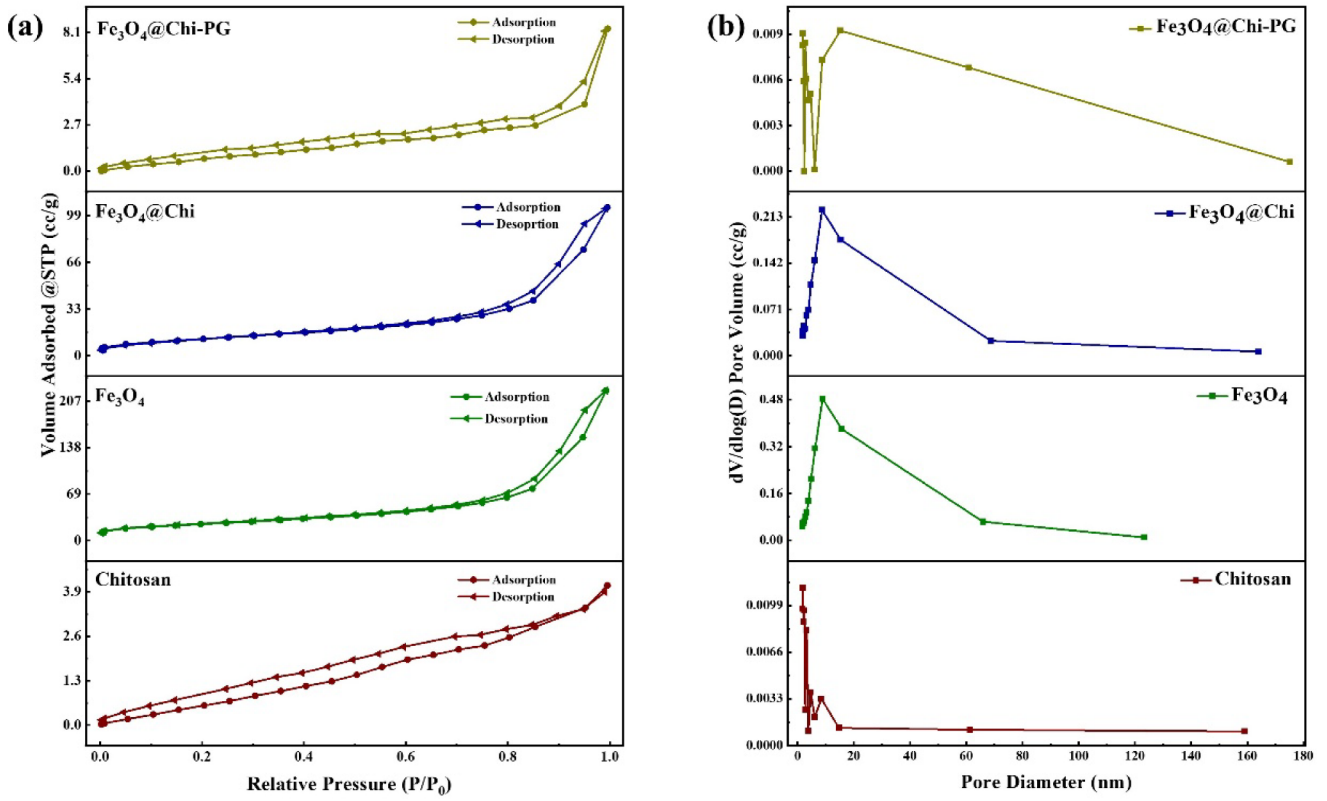

Figure 3. (a) Adsorption and desorption isotherms and (b) BJH pore size distribution curves of the synthesized materials.

Table 2. BET Surface Area, Pore Size, and Pore Volume Distribution of the Synthesized Samples

Sample	BET surface area (m^2/g)	Average pore size (nm)	Pore volume (cm^3/g)
Chitosan	4.104	3.078	0.006
Fe_3O_4	88.935	7.757	0.334
Fe_3O_4@Chi	45.471	7.134	0.162
Fe_3O_4@Chi-PG	3.127	7.428	0.013

Chi-PG (55.42 ± 1.06% and 29.28 ± 1.66% at 20 μg/mL). Nevertheless, Fe_3O_4@Chi-PG's RSA% significantly increased at higher doses (>20 μg/mL), minimizing this disparity and indicating a concentration-dependent release mechanism from the nanocarrier. The sustained rise in RSA% of Fe_3O_4@Chi-PG was due to the higher concentration of the loaded PG. IC_{50} values of PG and Fe_3O_4@Chi-PG were 8.67 ± 0.57 and 18.69 ± 1.54 μg/mL, respectively. Ascorbic acid had a reported RSA % of 98.0 ± 0.13% at 10 μg/mL, higher than the PG's (55.42 ± 1.06) and Fe_3O_4@Chi-PG's (29.28 ± 1.66) RSA% at the same concentration (Figure S2). With an IC_{50} value of 2.76 ± 0.26 μg/mL, ascorbic acid showed a higher capacity to scavenge radicals than both samples tested. Lower IC_{50} values indicate the strong antioxidant activity of the tested compounds. Thus, both samples showed strong antioxidant activity, indicating the potential to protect against the negative effects caused by free radicals. In a study conducted by Soltanzadeh et al.,[34] chitosan nanoparticle-loaded pomegranate peel extract showed 56% inhibition, which was significantly lower than that of the pure extract (85%). Similarly, Fawole et al.[78] reported an IC_{50} value of 15.88 μg/mL in a study that compared the antioxidant activity of pomegranate fruit peel extracts.

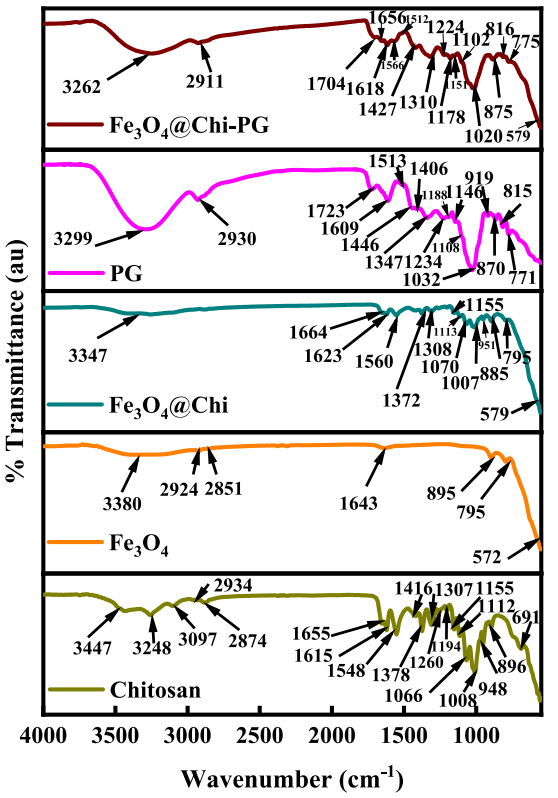

Figure 4. FT-IR spectra of synthesized chitosan, Fe_3O_4 NPs, extracted PG, and synthesized Fe_3O_4@Chi-PG.

Phenolic bioactive components in PG function to fight free radicals, which explains the extract's proven antioxidant ability.

https://doi.org/10.1021/acsomega.5c08001
ACS Omega 2025, 10, 50488−50510

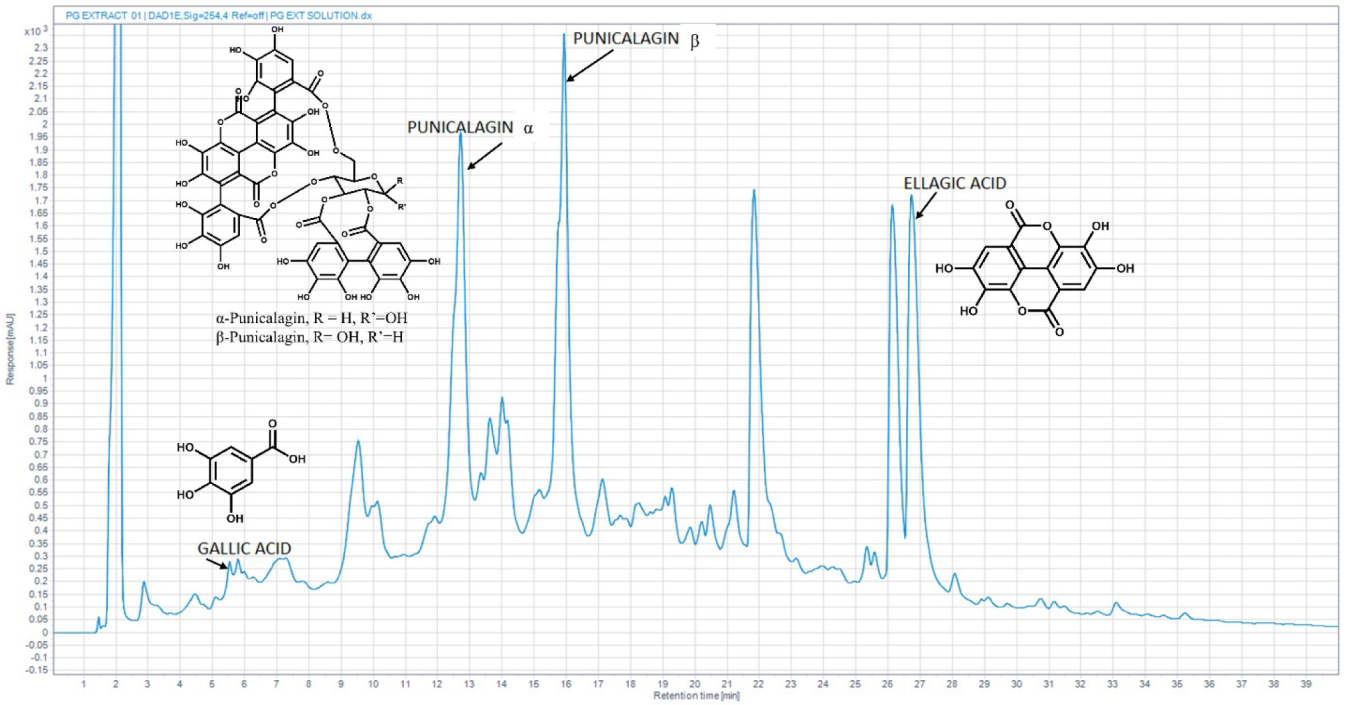

Figure 5. HPLC fingerprint of the *P. granatum* extract.

Table 3. Different Phenolic Compounds Were Identified in Methanolic Pomegranate Extracts by HPLC

Compound	Retention Time (min)	Area	Height	Relative Concentration %	References
Gallic Acid	5.520	1228.08	124.53	0.38	76
Ellagic Acid	26.716	37597.00	1536.27	11.68	74−76
Punicalagin α	12.701	35750.97	1505.07	11.11	74,76,77
Punicalagin β	15.917	41695.64	1897.85	12.95	74,76,77

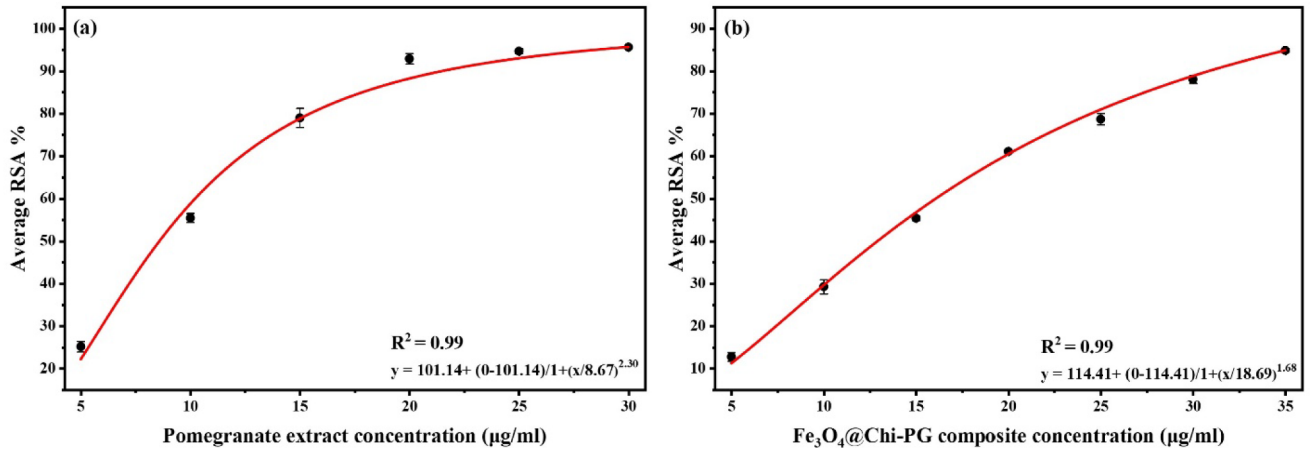

Figure 6. DPPH radical scavenging ability of (a) PG and (b) the Fe_3O_4@Chi-PG nanocomposite.

According to these findings, the antioxidant properties of pomegranates are mostly attributed to their total phenolic constituents. The scavenging capacity of pomegranate fruit is associated with its total phenolic, anthocyanin, and flavonoid content.[79] The natural polyphenolic chemicals in PG have antioxidant qualities, and the hydroxyl groups in the phenolic aromatic rings are one of the potential mechanisms of action.[80] These polyphenols' redox properties allow them to function as quenching agents against $1O_2$ and $3O_2$, neutralize free radicals, and dissolve peroxides, all of which contribute to their antioxidant action.[81] Among these compounds, the highly potent antioxidant activity of pomegranate is due to the presence of ellagitannins, which are responsible for most of the therapeutic properties, including anticancer, antibacterial, antiviral, and anti-inflammatory properties. Almost all parts of the fruit are found to exhibit anti-inflammatory properties, which are again linked with the radical scavenging ability. Punicic acid in pomegranate seeds was shown to be effective in fighting against cancer, diabetes, obesity, and cardiovascular diseases.[82,83] As demonstrated by Kohno et al.,[84] conjugated

https://doi.org/10.1021/acsomega.5c08001
ACS Omega 2025, 10, 50488−50510

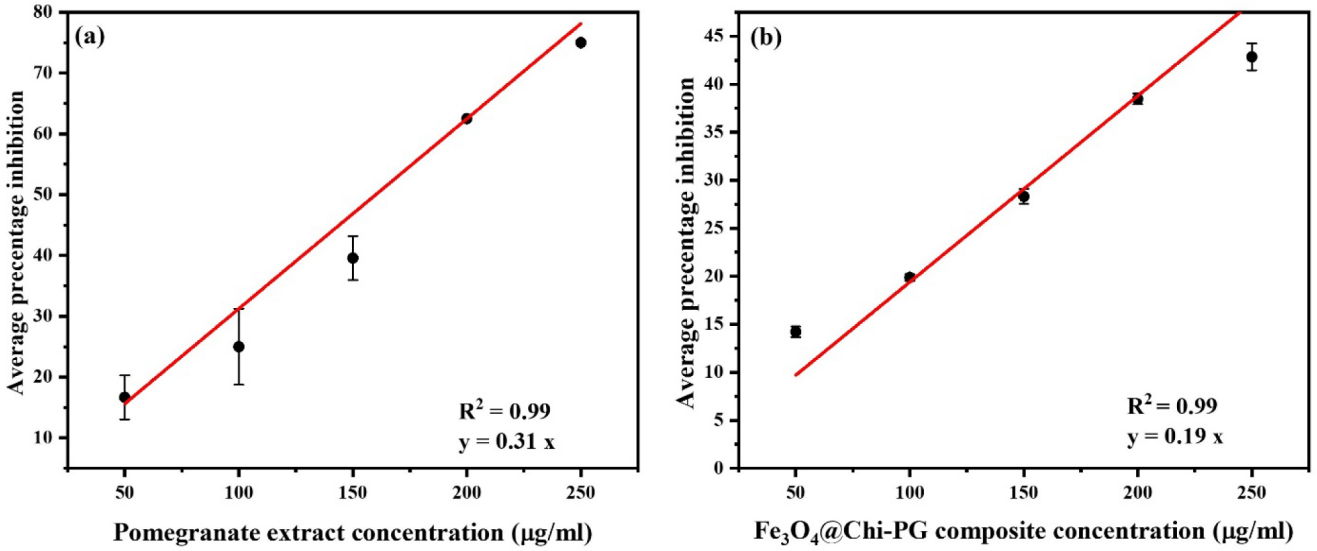

Figure 7. Anti-inflammatory activity of (a) PG and (b) the Fe_3O_4@Chi-PG nanocomposite.

linolenic acids in the seed oil can prevent or reduce the occurrence of multiple colon adenocarcinomas. Among the components of the pomegranate fruit, the peel was found to be the most abundant source of phenolic compounds, which is 2.8 times higher than that of the leaf extract, and according to Tehranifar et al.,[85] the peel extract exhibited an antioxidant capacity of 55.3%.

The antioxidant capacity of Fe_3O_4@Chi-PG is mainly due to the antioxidant properties of the loaded polyphenolic compounds. However, according to reports of Soleymanfallah et al. and Wan et al.[86,87] chitosan also has antioxidant properties. Low molecular weight chitosan has been shown to have a higher antioxidant activity than high molecular weight chitosan.[88] According to Hromis et al.,[89] low molecular weight chitosan with higher degrees of deacetylation has demonstrated stronger DPPH radical scavenging efficacy. Comparing low molecular weight chitosan with a degree of deacetylation >90% to that with a lesser degree, Alsharabasy[90] observed that the former one had greater scavenging properties. Fe_3O_4 NPs were also reported to have moderate antioxidant properties. In the study carried out by Ullah et al.,[91] Fe_3O_4 NPs exhibited 45 ± 3% DPPH radical scavenging ability with an IC_{50} value of 900 ± 3 μg/mL. Patra et al.[92] have reported that Fe_3O_4 NPs exhibited a very low DPPH RSA% of only 16.13% at 100 μg/mL compared to the positive control. Quercetin-loaded chitosan-grafted Fe_3O_4 NPs were reported to have a dose-dependent increase in DPPH RSA% with the increasing concentration of Fe_3O_4−chitosan.[93] Thus, using stabilizers, surface functionalization and coating, and doping with other metals have gained interest in the synthesis of Fe_3O_4 NPs with enhanced antioxidant activity. Since Fe_3O_4@Chi-PG was synthesized using higher molecular weight chitosan, its constituents have not significantly enhanced the drug composite's antioxidant capacity.

Polyphenolic compounds, which are loaded onto Fe_3O_4@Chi-PG via hydrogen bonding and hydrophobic interactions, should diffuse to the reaction media to interact with DPPH radicals. The complex matrix structure of Fe_3O_4@Chi, which will be discussed below, collectively ensures this diffusion of active compounds. Therefore, the protective effect of the delivery system in preventing the rapid leakage of polyphenolic compounds from the chitosan nanocomposite, thereby restricting their interaction with DPPH radicals, may be the reason for the lower RSA% value of Fe_3O_4@Chi-PG compared to PG. In contrast to PG, Fe_3O_4@Chi-PG showed lower initial RSA%, which gradually increased with concentration. Hence, the use of the Fe_3O_4@Chi system for the delivery of potent antioxidant compounds ensures the sustained release of active ingredients with significant antioxidant activity.

3.7. Anti-Inflammatory Activity. The egg albumin denaturation assay was conducted to evaluate the anti-inflammatory properties of PG and the Fe_3O_4@Chitosan-PG composite. The results are indicated in Figure 7 a,b respectively. The principal objective of the egg albumin denaturation assay is to determine if certain substances or agents may prevent or inhibit the denatured state of egg albumin in specific conditions, such as heat.[94]

Proteins become insoluble when they undergo denaturation, which is caused by a range of physical and chemical substances that alter their electrostatic forces and hydrophobic, disulfide, and hydrogen bonds. Inflammation results from the denaturation of intracellular materials and protein components within cells, which are linked to tissue damage. Therefore, it appears that a medicine or compound's capacity to prevent protein denaturation can be considered as a potential source against inflammatory reactions.[95]

The anti-inflammatory activity of PG and the Fe_3O_4@Chi-PG composite was evaluated in the concentration range of 50−250 μg/mL. A linear fit of the triplicate experimental absorbance data was used to determine the IC_{50} value, which is the concentration of the sample that can inhibit 50% of protein denaturation. Diclofenac sodium was used as the positive control. Both PG and Fe_3O_4@Chi-PG nanocomposites demonstrated a dose-dependent increment in the % inhibition activity. Percentage inhibition of PG varied from 16.67 ± 3.61% to 75.0 ± 0.00%, at 50 and 250 μg/mL concentrations, respectively. Fe_3O_4@Chi-PG exhibited a lower percentage inhibition compared to the pure extract, ranging between 14.23 ± 0.54% and 42.86 ± 1.39% in the same concentration range. The increment of the % inhibition was lower in the composite compared with the pure extract.

https://doi.org/10.1021/acsomega.5c08001
ACS Omega 2025, 10, 50488−50510

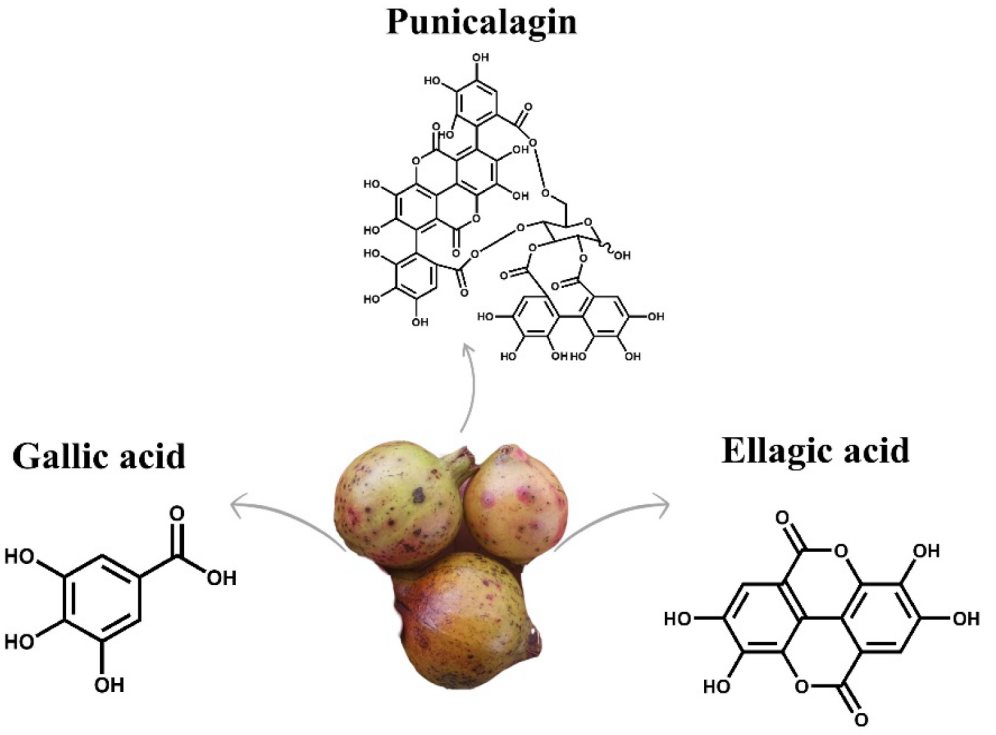

Figure 8. Phytochemicals in pomegranate extract.

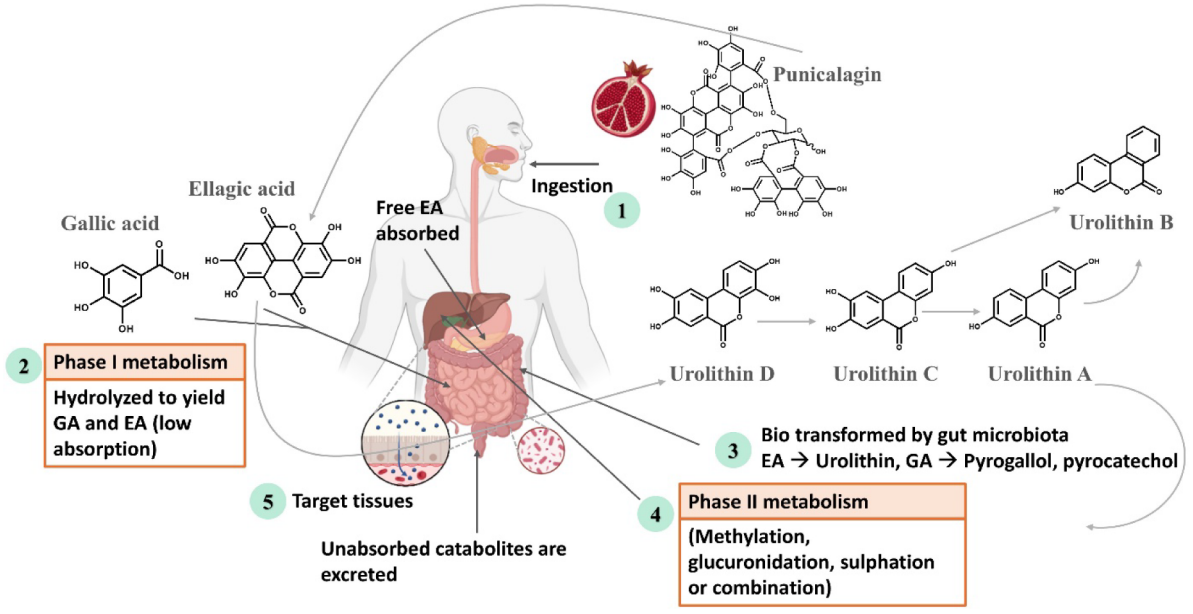

Figure 9. Metabolic pathway of bioactive compounds in*Punica granatum* extract.

Recorded IC_{50} values of the extract and nanocomposite were 160.0 μg/mL and 257.69 μg/mL, respectively.

The antioxidant and anti-inflammatory properties of PG were thought to be caused by the presence of phytochemicals such as hydrolyzable tannins (gallotannins and ellagitannins), their products, ellagic acid, or their common metabolites, urolithins, punicalagin, and polyphenols.[96] Reduction of inflammation regulators, including prostaglandin E2 and nitric oxide, and suppression of the nuclear factor-kappa B pathway are achieved by these compounds.[97] The pomegranate peel extract contains anti-inflammatory properties that improve liver enzyme activity and reduce liver inflammation by lowering proinflammatory activity and controlling inflammatory markers.[11,98] Sayed et al.[11] examined the role of the inflammatory enzyme cyclooxygenase (COX-2) in the inflammatory process. By inhibiting the production of prostaglandins, which are proinflammatory mediators, the pomegranate peel ethanol extract demonstrated an inhibitory impact against the inflammatory activity of the COX-2 enzyme. Ellagic acid/Na_2CO_3 was encapsulated in hollow zein nanoparticles using triethyl citrate as a natural plasticizer to deliver the EA by Ruan et al.[99] Overproduction of TNFα and IL1β, proinflammatory cytokines, was suppressed in the carrageenan-induced mouse paw edema model, indicating significant anti-

https://doi.org/10.1021/acsomega.5c08001
ACS Omega 2025, 10, 50488−50510

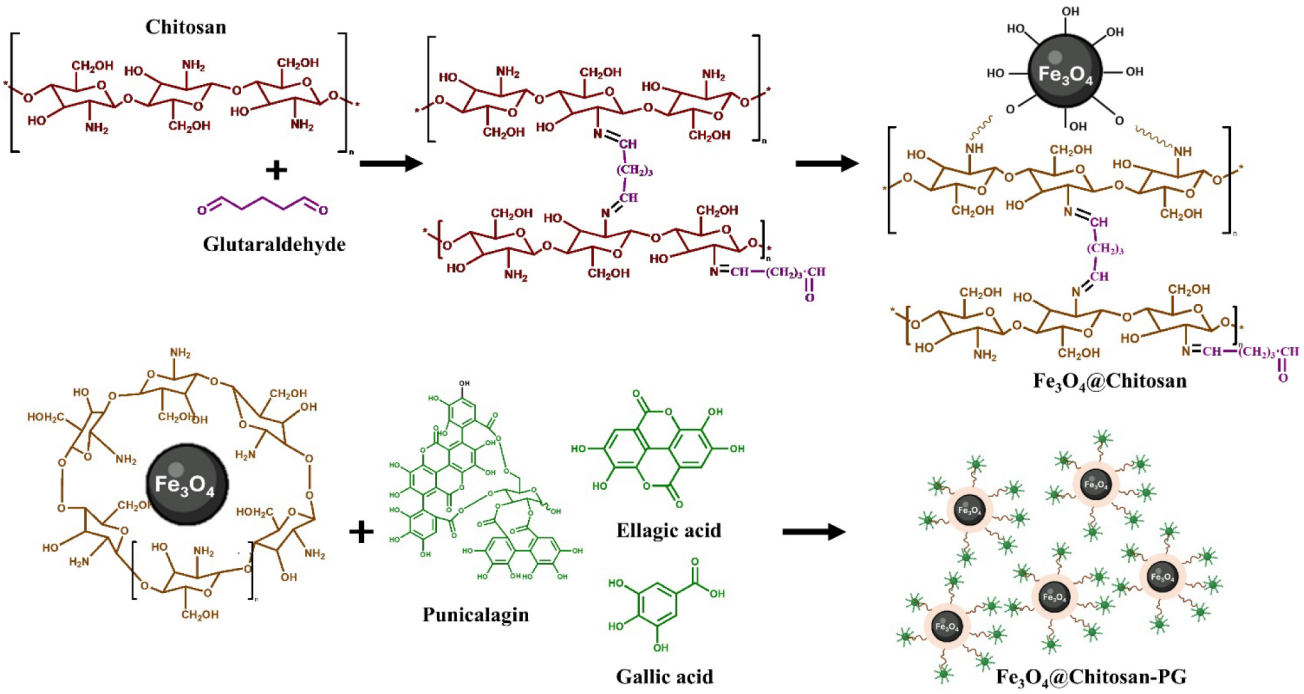

Figure 10. Synthesis of the Fe_3O_4@Chitosan-PG nanocomposite.

inflammatory activity. Several studies have indicated that Fe_3O_4 NPs possess proinflammatory activity. Fe_3O_4 NPs can alter the human neutrophil function by delaying apoptosis and inducing proinflammatory cytokines, as reported in the study conducted by Saafane & Girard.[100] In a study conducted by Bheemayya et al.,[101] Fe_3O_4 NPs were used as a catalyst for the synthesis of 3-(1,4,5-triaryl-1H-imidazol-2yl) quinolin-2-amines as COX-1 and COX-2 inhibitors with enhanced anti-inflammatory properties. Conversely, chitosan has been shown to have anti-inflammatory properties through regulating immune responses and lowering the synthesis of cytokines that promote inflammation.[102] However, in the present study, the mechanism of action of the composite is mainly due to the presence of the *P. granatum* extract. During the synthesis of the nanocomposite, PG has been loaded onto the surface of the delivery system, limiting the rapid interactions with the reaction media compared to the free extract. Thus, the lower % inhibition indicates that the delivery system successfully preserved the bioactive compounds without being subjected to rapid release. However, both samples have demonstrated significant anti-inflammatory activity, suggesting that the Fe_3O_4@Chi-PG nanocomposite delivery system effectively maintains the bioavailability of interested polyphenols.

3.8. Formulation of Fe_3O_4@Chi-PG Nanocomposite.

Numerous bioactive compounds are present in pomegranate fruit. The arils contain vitamin C, anthocyanins,[1] phenolic acids (ellagic acid and gallic acid), and hydroxycinnamic acids (chlorogenic acid, caffeic acid, and p-coumaric acid).[83] Secondary metabolites, including anthocyanins, phenolic acids, flavonoids, coumarins, vitamin E,[103] sterols, and punicic acid,[104] are present in pomegranate seeds. In terms of phytochemistry, pomegranate peel is distinguished by its abundance of polysaccharides, phenolic compounds, and flavonoids like quercetin, epicatechin, catechin, procyanidins, and anthocyanins.[105] Furthermore, the peel is abundant in hydrolyzable tannins, particularly ellagitannins. Up to 85% (w/w) of the tannins in pomegranate peel are punicalagin isomers, which are the most prevalent type of polyphenols. Punicalagin, ellagic acid, and gallic acid are the most significant active ingredients in pomegranate peel in this category, as shown in Figure 8.[106]

The metabolic pathways of the bioactive compounds in pomegranate extracts are shown in Figure 9. Ellagitannins are naturally unstable substances that can be hydrolyzed by enzymes and spontaneous processes. The gut bacteria in the distal small intestine and colon convert a greater percentage of ellagitannins and ellagic acid into urolithins and other metabolites. Since ellagitannins are precursors of ellagic acid and urolithins, which are thought to have systemic health advantages, it is imperative to increase their bioavailability. Therefore, compared to ellagic acid and gallic acid alone, increasing ellagitannins' bioavailability guarantees a higher potential for the formation of these advantageous metabolites. Even though ellagic acid is a metabolite of ellagitannins, it has low bioavailability; less than 1% of it is absorbed, and a large amount of it accumulates inside cells, lowering the systemic effects. This problem is indirectly resolved by making ellagitannins more bioavailable, which promotes the synthesis of urolithins and ellagic acid. Thus, increasing ellagitannin bioavailability guarantees a higher chance of systemic health advantages via urolithin synthesis.[107]

In order to preserve the qualities of the active ingredients, micro- and nanotechnology approaches have shown remarkable results in altering the pharmacokinetic properties, bioavailability, and stability of a variety of medications, including phytochemicals used in dietary supplements or cancer prevention. Solid dispersions, micro- and nanoparticles, inclusion complexes, self-emulsifying systems, and polymorphs are a few of the strategies used. El-Missiry et al.[108] have used alginic acid (ALG) for the synthesis of ellagic acid (EA)-ALG nanoparticles (NPs). Abd-Rabou and Ahmed[109] developed chitosan (CS) and polyethylene glycol (PEG) blended poly d-l-lactide-*co*-glycolide (PLGA) nanodelivery systems to encapsulate quercetin, ellagic acid, and gallic acid, and a gastric

https://doi.org/10.1021/acsomega.5c08001
ACS Omega 2025, 10, 50488−50510

dressing composed of chitosan-gelatin and pomegranate peel extract was fabricated by Jebahi et al.[110] Pomegranate extract-loaded solid lipid nanoparticles were prepared using cosurfactant, lecithin, by Badawi et al.,[111] with 40-fold improvement in anticancer activity against MCF-7breast, PC-3 prostate, and HepG-2 liver cancer cells compared to unencapsulated PG. Anwer et al.[112] have developed glycerosome-encapsulated *Punica granatum* with antibacterial effects for skin infections. A novel nanocarrier system consisting of silver NPs doped with pomegranate peel extract and hyaluronic acid was designed by El-Hamid et al.[113] to manage the *C. albicans* infection in wounds.

Polymeric magnetic composites have emerged as very promising materials in drug delivery due to their unique attributes, including rapid response and remote control capabilities. The use of Fe_3O_4 magnetic nanoparticles and polymers will produce magnetically sensitive polymers that can overcome the limitations of traditional polymers in remotely controlled release and targeted drug delivery.[37] In the current study, a chitosan−Fe_3O_4 delivery system was used to deliver the bioactive compounds in the pomegranate peel/seed extract to enhance the pharmacokinetic properties of the interested polyphenols, namely punicalagin, ellagic acid, and gallic acid. Chitosan can interact with Fe_3O_4 via electrostatic interactions and hydrogen bondings as it contains $-NH_2$ and −OH groups. These functional groups of chitosan can form H-bonds with the Fe_3O_4 surface.[42,114] Both chitosan and Fe_3O_4 change their surface charges according to the pH of the media. Hence, the electrostatic interactions can change according to the charge of the Fe_3O_4 surface and the protonation state of the NH_2 group in chitosan. Glutaraldehyde is added as the cross-linking agent in the nanocomposite synthesis. Glutaraldehyde can create interchain cross-linking via Schiff base formation of $-NH_2$ groups. Covalent C═N bonds can enhance the mechanical strength of the polymer network and form a 3D framework of chitosan chains around Fe_3O_4, preventing detachment.[115,116] Moderate cross-linking can create optimal loading and the release of the incorporated drug molecules, as the cross-linking affects the pore size of the polymeric network. Loading of the polyphenols of the PG occurs through the hydrogen bonding of the −OH groups of the polyphenols with the vacant −OH or $-NH_2$ groups of chitosan.[42] Hydrophobic interactions between aromatic rings of the polyphenols and the chitosan backbone can also occur in the loading process of PG to the delivery system. The schematic representation of the synthesis process of the Fe_3O_4@Chitosan-PG nanocomposite is depicted in Figure 10. Cellular uptake of the nanocomposite delivery system can occur via electrostatic interactions between the cationic nanocomposite and the negatively charged cellular membranes. The internalized composite will release the drug, and the biodegradable polymer will be eliminated by exocytosis.

Drug release mechanisms can be divided into four groups based on how a drug is released from a carrier: diffusion, ion exchange, dissolution, and erosion. Diffusion is the most basic form of drug release, where mass transport occurs according to the dosage form. However, it can be the predominant mechanism in some cases, while in others, it can be a part of the various mechanisms involved. Drugs are released from carrier systems through a combination of mechanisms involving more than one release mechanism.[117] Diffusional mass transport can be quantified using Fick's first law of diffusion, which indicates that the concentration gradient facilitates the process. Dissolution involves two steps: the initial release of the active ingredients from the surface of the carrier to the release media, followed by diffusion. The first phase of the release is faster, and hence, the concentration of the dissolving drug on the surface is equal to the solubility of the drug during the steady phase. Modification of the water-insoluble drug matrix with ionic functional groups that can swap ions from the release media is the principal mechanism in ion-exchange-based controlled release drugs. Drug molecules are bound to ionic sites through electrostatic interaction, and once the drug formulation is in the release media, drug molecules are exchanged with the ions of the same charge in the media.[118] According to Hillery and Park,[119] bioerodible matrix systems are sustained-release systems where the drug release is predominantly controlled by matrix erosion or degradation rather than diffusion or dissolution. When the rate of erosion is higher than the rate at which water penetrates the polymer, surface erosion takes place. It starts at the matrix/scaffold surface and gradually reduces the size of the matrix/scaffold from the outside to the inside. Since drug release is predictable and regulated, surface erosion is perfect for a variety of drug delivery applications. Furthermore, given that water-vulnerable drugs are shielded, a slow water penetration rate is optimal for drug delivery. Bulk erosion happens when water flows into the polymer's bulk, which breaks down the matrix uniformly. Hydrolysis can occur in the polymer, as the rate of water penetration is higher than the rate of erosion. This poorly predictable mechanism does not provide protection for the drug from the environment, making it a less-used mechanism for controlled delivery.[120]

Predicting the release rate and diffusion patterns of the active ingredients in delivery systems requires the application of mathematical models. This makes it possible to create new systems with more favorable release behaviors. As discussed above, the release of drugs from delivery systems can follow a combination of mechanisms. Understanding the release mechanism enables the prediction of the interactions between the system and the drug and creates room for modifications with more desirable release profiles. However, complete knowledge of the release mechanisms, which would allow for a precise estimation of release kinetics and molecular interactions, can only be achieved by precisely combining experimental results with the proposed mathematical models.[121] The selection of the mathematical model used to describe the release profile is also crucial, as many factors of the drug and carrier, including chemical and molecular composition, surface morphology, interactions, molecular weight, degradation rate, and size, can affect the release.[122] The most popular kinetic model in drug release studies is the Ritger−Peppas model, sometimes known as the power law. This model has been successfully used by numerous researchers for the past few decades to describe drug release by Fickian diffusion and anomalous transport.[122−126] In addition to this model, the Higuchi model,[127−129] zero-order model,[130−132] first-order model,[133−135] and Peppas−Sahlin model[136−139] have all successfully explained the drug release kinetics from polymer matrix systems. Thus, the release of the bioactive compounds from the Fe_3O_4@Chitosan-PG system was evaluated using these five drug release models based on the UV-spectrometry absorbance data.

Release of the polyphenols from the Fe_3O_4@Chi-PG nanocomposite system was evaluated by changing the pH of the release media within the range of 1−7.4. The pH range was

https://doi.org/10.1021/acsomega.5c08001
ACS Omega 2025, 10, 50488−50510

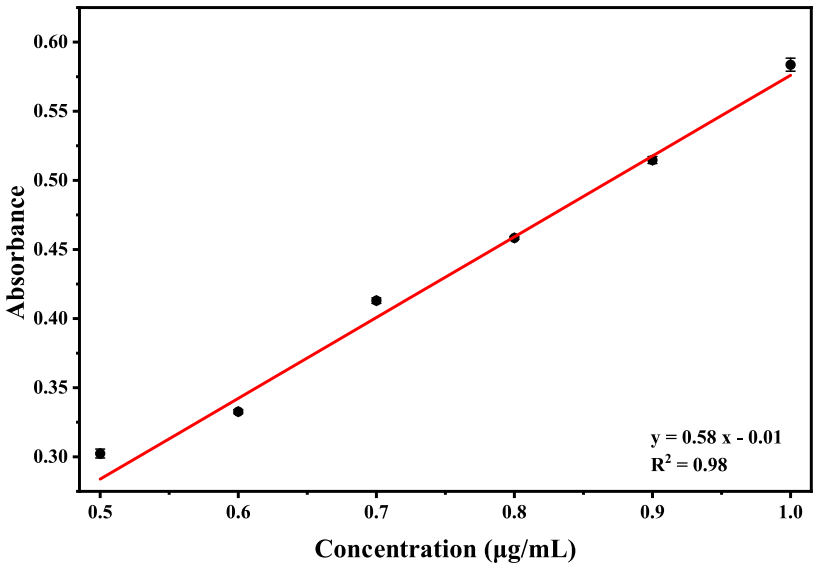

Figure 11. Calibration curve of PG.

selected considering the oral and IV delivery of the nanodrug composite. pH of the peripheral blood (7.4) and the pH range observed in the GIT are included within the selected range. pH of the GIT varies from acidic values in the stomach to ∼7.6 in the large intestines. In the normal state, the pH of the stomach varies between 1.5 and 2.0, whereas in the fasting state, it ranges between 3.0 and 5.0. The pH values of the small intestine and large intestine range between 5.0 and 6.5 and 6.4−7.6, respectively. Additionally, the release profile of PG's polyphenols, which are proven anticancer agents, was studied in pH values 5.5−6.8, mimicking the tumor macroenvironment. The pH values of the extracellular matrix of malignant tissues are reported to be lower than the normal extracellular pH (7.4) because of elevated glycolysis for ATP production, even at normal oxygen levels.[140,141]

3.9. Drug Encapsulation Efficiency % and Loading Degree %. The encapsulation efficiency of Fe_3O_4@Chi-PG was calculated by using the calibration curve (Figure 11). The concentration of unbound bioactive compounds was derived using the linear regression equation of the resulting calibration curve. EE% and LD% were calculated using eqs 4 and 5, respectively. The PG EE% in the Fe_3O_4@Chi-PG was reported to be 86.44% with a LD of 43.22% (Table 4). Naderi and

Table 4. EE% and LD% of Fe_3O_4@Chi-PG

PG concentration	Fe_3O_4@Chi ratio	EE%	LD%
3% (w/v)	1:1	86.44	43.22

Azizian[142] have developed carboxymethyl chitosan/Fe_3O_4 and $MnFe_2O_4$ nanocomposite hydrogels for the loading and release of curcumin, with loading efficiency ranging from 15.42−82.21% for the carboxymethyl chitosan/Fe_3O_4 composite. The loading efficiency was increased with the NP-to-chitosan ratio, where the highest loading efficiency of 82.21% was reported for the 1:2 ratio. However, in this study, the effect of the carrier system components on the loading efficiency was not considered.

3.10. Drug Release Studies. The absorbance data were collected in 15 min time intervals for 5 h at 360 nm using a UV−visible spectrophotometer to calculate the cumulative drug release % in each media composition. Cumulative release % of the different pH media compositions is represented in Figure 12 and Table S2. According to the results, the highest release was observed at pH 1, followed by pH 4, pH 5.5, pH 7.4, and pH 2.5. The lowest release was recorded at pH 6.7. pH of the media can alter the electrostatic interactions of the delivery system components by changing the surface charge of the Fe_3O_4 NPs and the protonation/deprotonation state of the $-NH_2$ groups. The Fe_3O_4 surface is strongly positive, whereas the NH_2 groups of chitosan are fully protonated (NH_3^+) in the media with pH 1.[143] Electrostatic repulsion of these charges makes the polymer−nanoparticle network loosely bound, facilitating the release of the loaded polyphenols at a higher rate. However, the H-bondings between some −OH groups of polyphenols and the Fe_3O_4 surface remain intact, despite the disruption of H-bondings by protonated Fe_3O_4 ($Fe-OH_2^+$). Punicalagin (pK_a ∼ 7−10)[144] and ellagic acid (pK_a ∼ 5.5−6.5)[27] remain in a neutral protonated state bound to the delivery system. The larger size of punicalgin and the low solubility of ellagic acid limit the release under this condition, but the protonated gallic acid (pK_a ∼ 4.4)[145] can diffuse easily owing to its smaller size. Although with protonated NH_2 groups and positive surface charge of Fe_3O_4, the release rate of the media with pH 2.5 is lower compared to pH 1 due to the lesser swelling state of the chitosan polymer. The protonated state of the OH groups in the polyphenol compounds remains the same as that in the pH 1 media, yet the slightly stabilized chitosan matrix reduces the release of the bioactive compounds, including the easily diffusible gallic acid. Chitosan matrix starts to partially deprotonate when the pH of the media changes to 4; thus, both $-NH_2$ and $-NH_3^+$ are present in the polymer matrix with $Fe-OH_2^+$/Fe−OH. Interested polyphenolic compounds remain bound to the matrix via H-bonding. The deprotonation of gallic acid creates electrostatic repulsion ($-COO^-$ and $Fe-O^-$), triggering a sudden increment of the drug release. Both the punicalagin and ellagic acid contribute to the release in minor amounts due to their larger size and lower solubility. The delivery system creates a tight polymer-NP network, with chitosan being more neutral with deprotonated $-NH_2$ groups and Fe−OH binding sites in the medium at pH 5.5. Fully deprotonated $-COO^-$ groups in

https://doi.org/10.1021/acsomega.5c08001
ACS Omega 2025, 10, 50488−50510

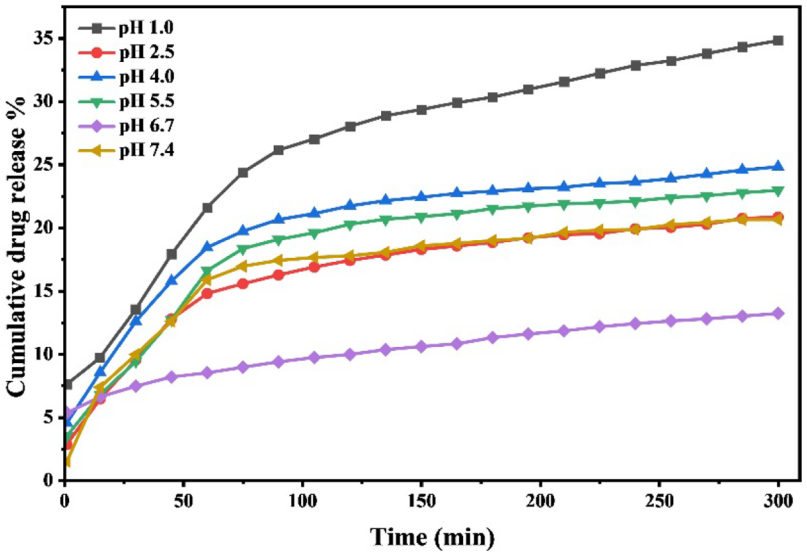

Figure 12. Cumulative drug release percentage of the synthesized Fe_3O_4@Chi-PG composite over time.

ellagic acid and deprotonated −OH groups of ellagic acid generate electrostatic repulsion forces with the tightened matrix, with a release profile similar to that at pH 4. But the neutral state of the chitosan matrix slows down the diffusion compared to the above scenario. Deprotonated chitosan ($pK_a \sim 6.4$)[146] and negatively charged $Fe_3O_4^-$ form a rigid matrix, slowing down the release of polyphenols in pH 6.7 release media. Carboxyl groups of gallic acid are fully deprotonated, which results in electrostatic repulsion, allowing the release of the active compounds. However, the partially deprotonated hydroxyl groups ($-O^-$) of ellagic acid are electrostatically attracted to the exposed Fe^{3+} sites (Lewis acids), forming inner-sphere complexes, limiting the release of the polyphenols. Further, π−cation interactions between the aromatic rings of the polyphenols and Fe^{3+} stabilize the binding of polyphenols to the matrix.[147] Punicalagin starts to contribute to the release in this media composition as the phenolic −OH starts deprotonating ($-O^-$, $pK_a \sim 7-10$). But the overall release rate is recorded to be lower as the chitosan matrix creates a hydrophobic, tightly packed matrix with less porosity. In the release media with pH 7.4, release of the bioactive compounds was reported to be higher despite the deprotonated chitosan matrix and the strongly negative Fe_3O_4 NP surface. The main cause of the swelling of the polymer chains is the hydration of the numerous hydroxyl (−OH) and amino ($-NH_2$) groups on chitosan.[148] Electrostatic repulsion between the negatively charged FeO_4 nanoparticle surfaces accelerates this relaxation. Additionally, the covalent cross-links that glutaraldehyde introduces produce a permanent steric hindrance that keeps the neutral chitosan chains from packing densely and maintains a baseline porosity. As a result of these processes, diffusion channels are formed for the release of bioactive compounds, aided by water uptake and matrix swelling. The release of gallic acid and ellagic acid is driven by the strong electrostatic repulsion from $Fe_3O_4^-$. These forces dominate the Fe^{3+} coordination and π−interactions, which were observed in the media with pH 6.7, as the full deprotonation degree is higher in the hydroxyl groups. But the metal-phenolate binding remains, limiting the release of the polyphenols compared with lower pH values. Even though the bulky structure restricts the release, the deprotonation of −OH groups of punicalagin enhances the repulsion forces within the matrix, allowing a detectable release in this media composition. Cumulative drug release data suggest that the synthesized nanocomposite delivery system enables the controlled release of the loaded polyphenolic compounds, driven by the swelling of the chitosan matrix and deprotonation-triggered release.

3.11. Release Kinetics. The release behavior of the drug depends on the interaction between the carrier and the delivery system. Conducting *in vitro* release studies helps to understand the release mechanisms, like diffusion, erosion, degradation, and dissolution, which control the release rate. The obtained release data were fitted into mathematical models considering the first 60% of cumulative drug release. The mathematical models used in the study are zero-order, first-order, Higuchi, Korsmeyer−Peppas (KP), and Peppas−Sahlin (PS) models. Kinetic models were fitted using nonlinear regression (OriginLab, Levenberg−Marquardt algorithm) and evaluated using R^2 (threshold ≥ 0.95). Model parameters of the models along with the corresponding R^2 values are mentioned in Table 5. The Korsmeyer−Peppas and Peppas−Sahlin models showed both superior fit ($R \geq 0.95$) and statistical significance in explaining the release kinetics in most of the media compositions, while the first order also showed some significance in some scenarios. Therefore, these models were taken into consideration in explaining the release mechanisms of the bioactive compounds from the Fe_3O_4@Chi-PG delivery system.

Diffusion-controlled systems are explained using Fick's laws, which fall under Fickian or non-Fickian diffusion. When the solvent diffusion time (t_D) is greater than the polymer relaxation time (t_R), Fickian diffusion occurs, and non-Fickian diffusion occurs when $t_R \gg t_D$.[149] Based on this principle, the Korsmeyer−Peppas model was developed. This equation could accurately describe drug release in the hydrogel and other polymeric materials. This model is useful for complex mechanisms, such as when several release mechanisms are coupled or when diffusion (Fickian diffusion) and Case II transport (non-Fickian) are combined.[70] This model, which is often referred to as the modified power-law model, uses the following equation to illustrate an exponential relationship between the drug release percentage and time (t):

https://doi.org/10.1021/acsomega.5c08001
ACS Omega 2025, 10, 50488−50510

Table 5. pH-Dependent Drug Release Kinetics Data of Fe_3O_4@Chi-PG Fitted with the Korsmeyer–Peppas Model, Peppas–Shalin Model, Higuchi Model, Zero-Order Model, and First-Order Model (Model Parameters and R^2 Values)

Model/parameters	pH 1	pH 2.5	pH 4	pH 5.5	pH 6.7	pH 7.4
Korsmeyer–Peppas						
k_P	0.16	0.19	0.23	0.19	0.28	0.08
n	0.33	0.30	0.27	0.30	0.22	0.46
R^2	0.95	0.96	0.94	0.92	0.95	0.98
Peppas–Sahlin						
k_D	3.48	3.58	5.87	4.41	2.57	0.10
k_R	1.36	0.00	0.00	0.00	0.64	1.60
m	0.25	0.32	0.27	0.30	0.19	0.23
R^2	0.95	0.97	0.93	0.92	0.96	0.97
Higuchi						
k_H	2.29	1.38	1.68	1.75	0.81	1.40
R^2	0.90	0.89	0.66	0.86	0.60	0.97
Zero						
k_0	0.10	0.06	0.05	0.07	0.02	0.09
R^2	0.89	0.77	0.67	0.73	0.96	0.89
First						
k_1	0.02	0.02	0.03	0.02	0.70	0.07
R^2	0.90	0.96	0.96	0.96	0.23	0.98

$$M_t/M_\infty = Kt^n$$

In the equation, K is the release rate constant, which is dependent on the geometry and structural characteristics of the delivery system. The release exponent (n) is used to describe the release mechanism, where Fickian diffusion occurs when $n \leq 0.45$, anomalous or non-Fickian diffusion occurs when $0.45 < n < 0.89$, super case II occurs when $n > 0.89$, and zero-order release occurs at $n = 1$. The rate of diffusion in Fickian diffusion is greater than the rates of swelling and relaxation of polymers. As a result, the drug's diffusion influences the release rate. In contrast, swelling and polymer relaxation occur in anomalous (non-Fickian) transport.[118]

The nonlinear kinetic model fits of the KP model are demonstrated in Figure 13 along with other parameters. Release of the media with pH 1, 2.5, 6.7, and 7.4 is fitted well with $R^2 \geq 0.95$, indicating the suitability of the KP model in explaining the drug release mechanism. According to the model parameters, the release behavior of the polyphenols in the pH range between 1 and 6.7 aligns with the Fickian diffusion ($n \leq 0.45$). As indicated by the n value, anomalous or non-Fickian diffusion occurs at pH 7.4 ($n = 0.46$). At pH 1, chitosan protonation (NH_3^+) facilitates polymer swelling via electrostatic repulsion between polymer chains, leading to increased porosity in the matrix. This allows the faster diffusion of the polyphenols. Additionally, this results in weaker H-bonding with the polyphenols, allowing the faster release. Gallic acid can easily diffuse owing to its lower molecular weight, whereas the punicalagin release rate is lower due to the steric hindrance. Ellagic acid has a low solubility compared to gallic acid, yet the swelling of the matrix aids the diffusion. Fe_3O_4 is stable under pH 1 media, and the chitosan swelling governs the release mainly. The relatively high k_P value indicates a faster release rate following Fickian diffusion. The chitosan polymer matrix remains protonated in the pH 2.5 media as well, but the swelling is reduced compared to pH 1, resulting in a reduced release rate. Electrostatic repulsion contributes to the polymer swelling to some extent. H-bondings with the polyphenols are partially restored due to the reduced charge density. These interactions retain the polyphenols (punicalagin) more strongly than in the pH 1 media, but the gallic acid and ellagic acid can diffuse via the swollen matrix. Fe_3O_4 is less protonated and can interact with the negatively charged OH groups of polyphenols, slowing the release rate. Fickian diffusion is the predominant release mechanism with an n value of 0.30 and a more sustained release behavior. The balanced swelling and H-bond formation ensure that the loaded polyphenols remain in the delivery system. At pH 4, the release rate is higher compared to those of the previous scenarios. Partial protonation of the chitosan

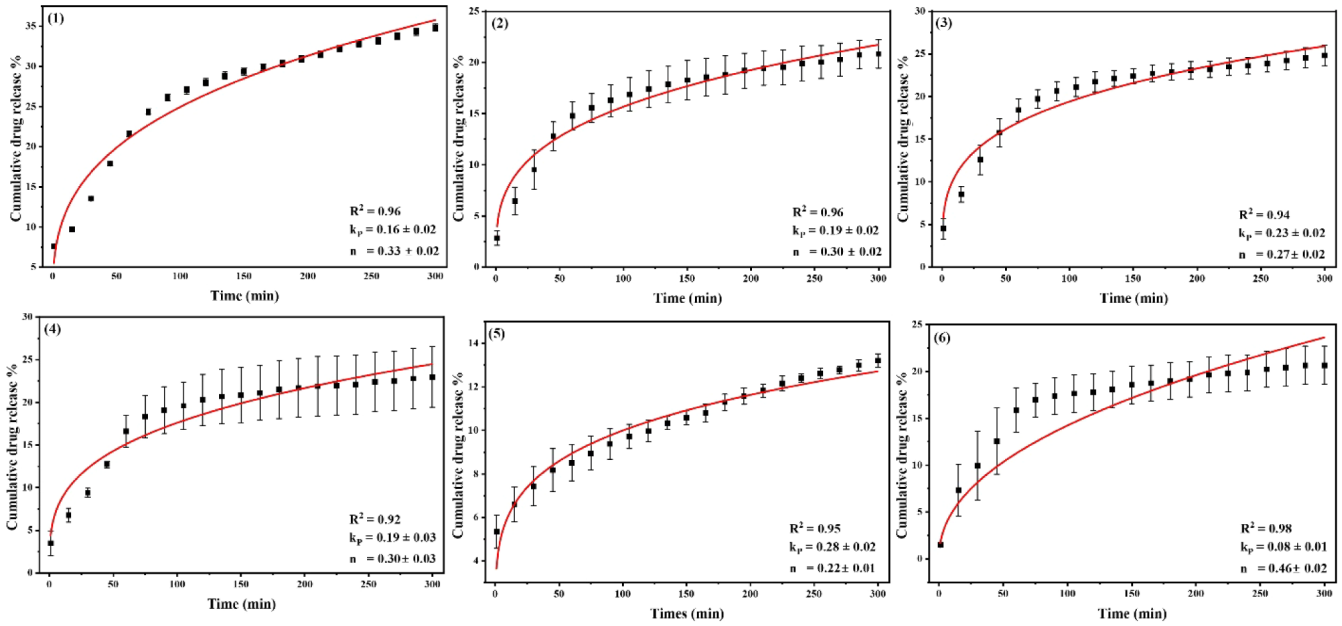

Figure 13. Fitted %CDR data for Korsmeyer–Peppas model of the Fe_3O_4@Chi-PG under varying media conditions: (1) pH 1, (2) pH 2.5, (3) pH 4, (4) pH 5.5, (5) pH 6.7, and (6) pH 7.4.

https://doi.org/10.1021/acsomega.5c08001
ACS Omega 2025, 10, 50488–50510

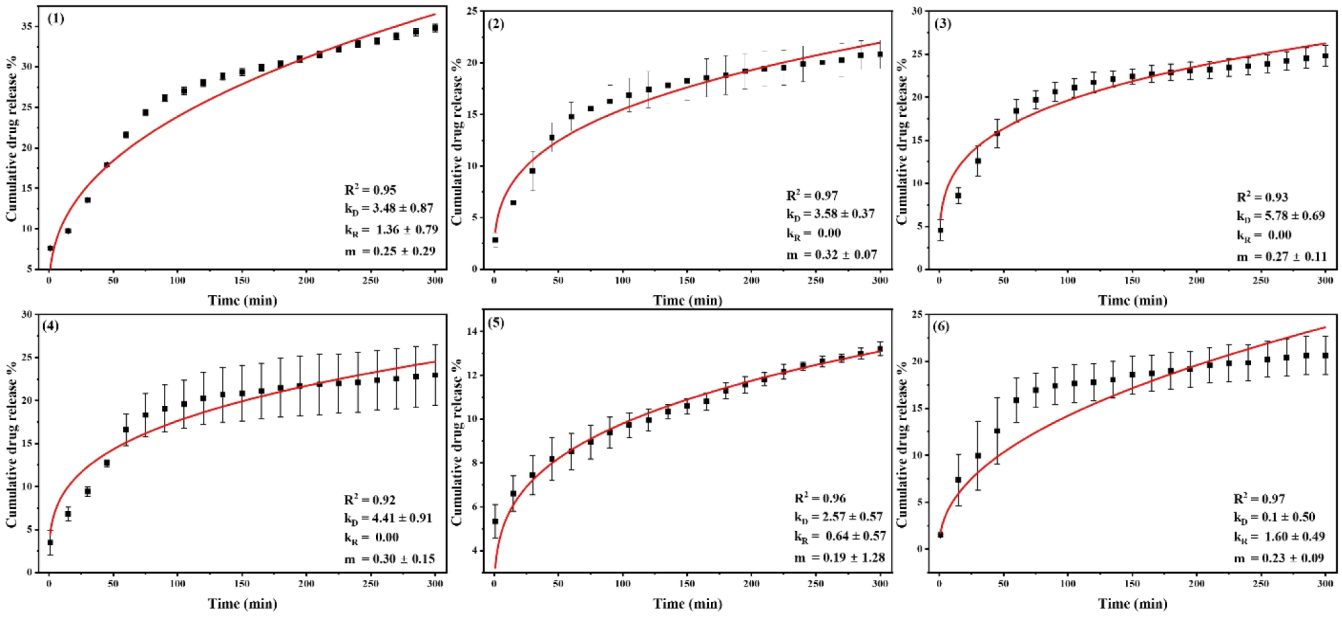

Figure 14. Fitted %CDR data for Peppas–Sahlin model of the Fe_3O_4@Chi-PG under varying media conditions: (1) pH 1, (2) pH 2.5, (3) pH 4, (4) pH 5.5, (5) pH 6.7, and (6) pH 7.4.

matrix collapses the polymer matrix, creating transient pores. Loaded polyphenols can diffuse easily through this structure. Specifically, lower molecular weight (MW) gallic acid and moderate MW ellagic acid benefit mostly from the transient pores. Higher MW punicalagin release is moderate to lower under this condition, despite weaker H-bonding and better solubility. Fe_3O_4 remains stable as in previous cases, with the ability to form weak electrostatic interactions with hydroxyl groups of polyphenolic compounds. With partial deprotonation, the chitosan matrix shrinks more, and the electrostatic repulsion forces become weaker between the polymer chains at pH 5.5. Hydrogen bonding of the polyphenols dominates over repulsion, but the micropores remain in the partially collapsing polymer. Though Fe_3O_4 remains neutral, weak coordinative bonds of the Fe_3O_4 surface (Fe^{3+} with polyphenol − OH groups) reduce the release of bulky phenolic compounds like punicalagin. The moderate release rate is due to the shrinkage of the polymer matrix, resulting in tortuosity, where the active compounds have to take a longer path to diffuse out. The increment in the n value (n = 0.30) is not due to the polymer erosion or relaxation but is due to the tortuosity effect of the shrunken matrix. Fickian diffusion remains the predominant mechanism of release, but the comparatively low R^2 (R^2 = 0.94 and 0.92) suggests there could be deviations from the pure Fickian diffusion release at pH 4 and pH 5.5 media compositions, respectively. As chitosan can form stronger H-bonds with the polyphenols compared to the lower pH media, the release rate is lower, with gallic acid being the major contributor to the release via diffusion. The model fit for the first-order model is remarkably higher at pH 5.5 and 4 compared with the KP model, suggesting that polyphenol solubility (dissolution) plays a role in the release. This transition from Fickian diffusion to combined diffusion and dissolution effects proposes that the system is suitable for sustained delivery. The release at pH 6.7 is governed by strong Fickian diffusion, unlike that at pH 5.5. The chitosan ($pK_a \sim$ 6.4) is fully deprotonated, and the polymer retains microporosity due to the hydrophobic interactions within the chains and the weakened H-bonding with polyphenols. The Fe_3O_4 surface becomes slightly negative in charge and weakly interacts with the ionized polyphenols. Fully ionized and partially ionized COO^- groups of gallic acid, ellagic acid, and punicalagin contribute to these interactions, slowing the release compared with acidic media compositions. However, the release rate is higher compared to pH 5.5, demonstrating a Fickian diffusion controlled by the ionization of the polyphenols, with no tortuosity effects. The molecules are diffused, overcoming the chitosan matrix contractions, because of ionized COOH groups, which are repelled by the matrix. Conversely, anomalous transport occurs in pH 7.4 media with a reported n value of 0.46. As explained in the CDR% analysis, swelling of the polymer can happen with water uptake through hydrophilic pores. Gradual relaxation of the dense matrix of chitosan over time and the stronger electrostatic repulsive forces of negatively charged Fe_3O_4 on the ionized polyphenols direct the release of these compounds from the matrix. The release rate driven by diffusion was reported to be lower at pH 7.4, as the relaxation is proven to be part of the release mechanism, indicated by the PS model fit. Interestingly, punicalagin actively participates in the ionization under this pH, suggesting an enhanced release of the bioactive compound compared to that of other media compositions.

The PS model does not determine the release mechanisms depending solely on Fickian diffusion, but it provides a detailed analysis of the release mechanisms, quantifying the contributions of both Fickian diffusion and relaxation of polymer matrices. The first term of the model equation (eq 11) indicates the contribution of diffusion, whereas the second term denotes the relaxational contribution. Term m indicates the Fickian diffusion exponent; hence, when the release is governed by Fickian diffusion, the m value of the PS model should be equal to the n value of the KP model. In contrast, when both Fickian diffusion and relaxation contribute to the release of active compounds, exponents n and m are not equal.[122] Figure 14 shows the kinetic model fits of the PS model and the respective model parameters. The modification

https://doi.org/10.1021/acsomega.5c08001
ACS Omega 2025, 10, 50488−50510

of the model equation (eq 12) can be used to determine the ratio between relaxation and diffusion. When R/F = 1, both mechanisms contribute equally to the release of the drug, diffusion predominates when R/F < 1, and relaxation contributes more to the release when R/F > 1.[150] Figure S3 represents the R/F against time plots, which were calculated using the model parameters and CDR% data.

In media with pH = 1, the relaxational contribution to release is due to the protonation of the chitosan matrix, as explained in the KP model data. Swelling of the matrix creates transient pores that enhance the release beyond pure diffusion. This high protonation causes the polymer to swell, leading to chain disentanglement and weakening of the bonds with the polyphenols. As represented in Figure S3, diffusion dominates the release, resulting in a burst release of the loaded polyphenols, but after the first hour, relaxation contributes to the sustained release. According to the model fits, relaxational contribution k_R was reported to be zero in media compositions with pH 2.5, 4, and 5.5. Chitosan is at a partial protonation state at pH 2.5, but less swelling is expected, as the electrostatic repulsion is weaker because of fewer $-NH_3^+$ groups. However, the PS model has not captured relaxation as a leading factor to the release mechanism since the contribution is not significant compared to the pH 1 media. Moderate swelling of the polymer can occur because of the partially protonated NH_3 groups, but the PS model can detect relaxation only if it contributes significantly to mass transport. As explained in the KP model, strong Fickian diffusion governs the release at pH 4 ($k_R = 0$), and the increment in the n value at pH 5.5 is not due to polymer relaxation but because of the formation of micropores in the shrunken hydrophobic matrix. These findings are further confirmed by the model parameter data, where the n values of the KP model are similar to the m values of the PS model in each scenario. Therefore, the predominant release mechanism is revealed to be Fickian diffusion in pH 2.5, 4, and 5.5 media compositions. Both Fickian diffusion and relaxation contribute to release at pH 6.7, with relaxation being less prominent. A fully protonated chitosan matrix facilitates the release of polyphenolic compounds by diffusion through micropores and the ionization of functional groups. Chitosan's near-neutral state forms a balanced swelling/shrinking state with detectable relaxation. Additionally, the positive surface charge of Fe_3O_4, which stabilizes the matrix in acidic media, is neutral at this pH, making weak interactions with chitosan/polyphenols, allowing polymer loosening. Unlike at pH 2.5, where diffusion is fast and prominent compared to swelling, at pH 6.7, diffusion is slower, permitting the polymer chains to create dynamic rearrangements. The significance of relaxation is very low, which is further proven by the R/F plot, where the values are <0 throughout the entire release period. Conversely, relaxation is the major contributor to the release mechanism at pH 7.4 ($k_R = 1.6$), where gradual relaxation occurs with water uptake to the hydrophobically collapsed polymer. Chitosan–Fe_3O_4 adhesion becomes weaker with a negatively charged surface, promoting polymer relaxation. Electrostatic repulsion between ionized polyphenols with the matrix components, specifically Fe_3O_4, and pore formation are responsible for the release of polyphenols under pH 7.4 media. The KP model indicated that anomalous transport is responsible for the release, with diffusion being a part of it. In accordance with R/F graphs, relaxation is the leading force of polyphenol release, where the R/F ratio was reported to be >1. Furthermore, the PS model fits ensure that the n value ($n = 0.46$) of the KP model represents the relaxational contribution, but not the erosion of the drug delivery system. The model fits reveal that the release of the interested bioactive compounds is governed through time-dependent polymer relaxation, which is crucial for creating pH-sensitive delivery systems.

Figures S4–S6 represent the model fits of the Higuchi, zero-order, and first-order models, respectively. The nonlinear model fits of the Higuchi model indicate less significant R^2 values, as depicted in Table 5. The following assumptions should be considered when applying the Higuchi model equation to interpret the release of drugs from delivery systems: a) a homogeneously loaded drug is constantly diffused from the matrix; b) the initial drug concentration is significantly higher than the drug solubility; and c) the formulation's thickness exceeds that of the drug molecules. The drug diffusion coefficient is assumed to be constant, and the model disregards any swelling or relaxational contribution of the polymer carrier.[149,151] However, as shown in the results, diffusion is not the sole governing factor of the release mechanism. Initial burst effects, swelling, relaxation, and changes in the polymer matrix were exhibited in the delivery system under varying pH media compositions. Thus, interpreting the results based on the Higuchi model alone can lead to erroneous conclusions about the release behavior. Combining the results of the Higuchi model with those of others will be beneficial when multiple mechanisms are responsible for the drug release of complex systems. However, k_H values of the Higuchi model align with the CDR% data and release mechanisms discussed in the KP and PS models in some instances. pH 1 has the highest rate due to the initial burst effect, facilitating the diffusion. The lowest k_H value is recorded for the media with pH 6.7, as the swelling or chain rearrangements are not considered in the Higuchi model when interpreting the release behavior. Lower R^2 values of the model indicate poor alignment of the actual release behavior with the assumptions of the Higuchi model.

Drug release at a consistent rate across the lifetime of the drug is described by a zero-order system. It is unaffected by the drug concentration in the system. Ideal zero-order systems release medications at the same rate as those that are taken out of the body when they are in equilibrium. Consequently, the body's total cumulative dose is decreased. As a result, it permits consistent plasma concentrations and accurate dosing, decreasing side effects and lowering the possibility of long-term toxicity. However, because it requires a large and costly system with a restricted temporal range and inconvenient use, the manufacture of devices with optimal zero-order kinetics is still limited.[152] According to the first-order model, the quantity of drug released into the system determines the release rate of the drug over time. The concentration gradient between the matrix and the medium's solid–liquid interface determines the release rate in this model.[153] For the zero-order model, relatively low R^2 values are recorded, whereas, in contrast, considerably higher R^2 values are reported for the first-order model in most of the media compositions. When the release is based on the dissolution of the drug, which directly correlates with concentration (pH 2.5, 4, and 5.5), or matrix effects, such as relaxation, where the remaining amount of the drug is proportional to the drug exposed (pH 7.4), the first-order model is fitted well with the data ($R^2 \geq 0.95$). However, at pH 1, where the extreme swelling of the polymer facilitates diffusion, and at pH 6.7, where the system is at a transitional

https://doi.org/10.1021/acsomega.5c08001
ACS Omega 2025, 10, 50488–50510

phase, which is neither dissolution-limited nor relaxation-dominated, the first-order model fails to fit the release data.

Overall, a combination of mechanisms, including diffusion, polymer relaxation, swelling, and drug dissolution, contributes to the release of the loaded ellagic acid, gallic acid, and punicalagin from the Fe_3O_4@chitosan delivery system. Fickian diffusion is the major contributor to the release of polyphenols in all the media compositions except at pH 7.4, where water uptake, pore formation, and ionization-aided electrostatic repulsion facilitate the drug release via polymer relaxation. Under strongly acidic conditions (pH 1), swelling of the polymer matrix is significantly higher with the protonation of NH_3^+ groups of the chitosan biopolymer, but deprotonation occurs with the increment of the pH. This reduces the electrostatic repulsion between the polymer chains, creating a tightly packed, hydrophobic structure that leads to decreased swelling and increased stability at neutral or alkaline pH levels. Transient pore formation occurs with the collapse of the chitosan matrix (near the pK_a value), enabling the release of the polyphenols from the matrix despite the stronger H-bond formation with the chitosan polymer, compared to acidic media. Fe_3O_4 acts as a matrix stabilizer in acidic media compositions, but when the pH > 6.5, the negatively charged surface of the magnetite NPs allows polymer relaxation. Hence, electrostatic repulsive forces between the NPs' surface and the ionized carboxyl groups of the phenolic compounds assist the diffusion of these compounds to the release media. Lower MW gallic acid is easily diffused in all of the pH media compositions, contributing to the release, followed by the moderate MW ellagic acid. Punicalagin, being a bulky molecule, is released under near-neutral pH conditions, aided by the repulsive forces of the matrix. Therefore, the pH-responsive sustained release behavior of the designed delivery system is ideal for the delivery of targeted polyphenols to the specific sites.

It is crucial to highlight that CDR% in this study reached only up to a maximum level of 35% due to the non-sink conditions and the small volume cuvette systems used. Future studies should focus on optimizing the drug loading capacity of the delivery system and evaluating the release behavior under sink conditions to obtain a complete release profile. The drug release study was designed to perform a fundamental and preliminary investigation to demonstrate the pH-responsive behavior of the Fe_3O_4@Chi-PG delivery system, rather than to stimulate physiological conditions. Furthermore, as reported by Nazir et al., Zhang et al., and C. Zhang et al.,[154−156] the release of drugs targeting the GIT and targeted tissues (malignant) is evaluated over a prolonged period, stimulating the extracellular environment parameters. The release profile was plotted based on the initial release kinetics of Fe_3O_4@Chi-PG to identify the dominant release mechanisms under different pH conditions, which is a necessary first step to understand the release behavior.

Glutaraldehyde was used as the cross-linker during the synthesis of Fe_3O_4@Chi-PG delivery system, as it can form stable covalent networks with chitosan. Although glutaraldehyde is the most commonly utilized cross-linker in biodegradable hydrogels,[157,158], there is significant evidence of its cytotoxicity.[159,160] This study did not assess the potential cytotoxic effects of the Fe_3O_4@Chi composite, including the residual effects of the cross-linker, but these are documented as a primary limitation. Nevertheless, according to several studies, chitosan and Fe_3O_4 nanoparticles both show better biocompatibility with low cytotoxic profiles.[161,162] However, a thorough safety evaluation of this particular composition via *in vivo* studies is still necessary for further biomedical applications.[163]

4. CONCLUSIONS

The delivery system composed of Fe_3O_4NPs and chitosan was developed to deliver polyphenolic compounds derived from PG with an encapsulation efficiency of 86.44%. HPLC analysis was conducted to determine the presence of the interested bioactive compounds, namely gallic acid, ellagic acid, and punicalagin. The XRD analysis revealed that the corresponding peaks of chitosan and Fe_3O_4 were present in the composite materials, suggesting successful coupling of the synthesized materials. Loading of Fe_3O_4@Chi with the PG extract was confirmed via the FT-IR spectrum, which indicated the presence of functional groups related to polyphenolic compounds in Fe_3O_4@Chi-PG. BET analysis revealed an extensive reduction of the BET surface area and pore volume in Fe_3O_4@Chi-PG, confirming the loading of PG. Similarly, SEM images demonstrated that the macropore structure of the chitosan matrix was covered by the incorporation of Fe_3O_4 and pomegranate extract in Fe_3O_4@Chi-PG. The reported IC_{50} values for the DPPH RSA% of PG and Fe_3O_4@Chi-PG were 8.67 ± 0.57 and 18.69 ± 1.54 μg/mL, respectively. Results of the egg albumin denaturation assay indicated that the IC_{50} values of the PG and Fe_3O_4@Chi-PG were 160.0 and 257.69 μg/mL, respectively. Drug release kinetics results indicate that KP and PS models were fitted well in most of the release media compositions, while the first-order model showed significance at some compositions. According to the n values of the KP model, quasi-Fickian diffusion was the predominant release mechanism of polyphenolic compounds in all the pH media compositions tested except for the media with pH 7.4, where non-Fickian diffusion occurs (n = 0.46). At lower pH values, swelling occurs via the protonation of NH_2 groups in chitosan, which creates a faster release with a burst effect, specifically at pH 1. When the pH was increased above pH 4, deprotonation of the chitosan creates a rigid network with fewer electrostatic repulsions. Fe_3O_4 stabilizes the polymer network at lower pH values, controlling the burst effects in the release. However, when the surface of Fe_3O_4 becomes more negative with the increase of pH, Fe_3O_4 contributes to the release of the loaded polyphenols via relaxation of the polymer network (pH 7.4). Polyphenol compounds are bound to the nanocarrier via H-bonds, and the release is mainly dominated by the molecular weight of the compounds, repulsive forces created by the ionization of OH and COOH groups with pH increment, and the polymer rearrangements. Relaxation is a major contributor to the release at pH 7.4, as indicated by the PS model parameters (R/F > 1). However, the contribution of relaxation to the release of polyphenols at pH 2.5, 4, and 5.5 was negligible according to the parameters (k_R = 0). Dissolution of the compounds was also reported to be responsible for the release at pH 4, 5.5, and 7.4 (first-order release) when the concentration of the drug correlates with diffusion due to matrix effects. Therefore, the punicalagin/ellagic acid/gallic acid-loaded Fe_3O_4@Chi nanocomposite exhibits pH-responsive release behavior according to the results. The use of higher molecular weight chitosan with reduced water solubility, the absence of cytotoxicity assessments of the drug carrier system and its components, and the absence of *in vivo* tests to assess the delivery system's bioavailability and safety are some of the

https://doi.org/10.1021/acsomega.5c08001
ACS Omega 2025, 10, 50488−50510

drawbacks of this study. To evaluate the pharmacokinetics and therapeutic efficacy of this delivery system, further *in vivo* evaluations are required. Future studies should include more comprehensive cytotoxicity evaluations and long-term toxicity studies to validate the proposed drug carrier's clinical safety and biocompatibility.

■ ASSOCIATED CONTENT

Data Availability Statement

The data sets used and/or analyzed during the current study are available from the corresponding author on reasonable request.

Supporting Information

The Supporting Information is available free of charge at https://pubs.acs.org/doi/10.1021/acsomega.5c08001.

HPLC spectra of the standards, DPPH RSA% of positive control, FT-IR vibrational bands and their corresponding functional groups, CDR% of Fe_3O_4@Chi-PG, R/F values of the Peppas−Sahlin model, and fitted %CDR data for the Higuchi model, zero order and first order of the Fe_3O_4@Chi-PG (PDF)

■ AUTHOR INFORMATION

Corresponding Author

Charitha Thambiliyagodage − *Department of Applied Sciences, Faculty of Humanities and Sciences, Sri Lanka Institute of Information Technology, Malabe 10115, Sri Lanka*; orcid.org/0000-0003-0906-4441; Email: charitha.t@sliit.lk

Authors

Ravimal Rukshan − *Department of Applied Sciences, Faculty of Humanities and Sciences, Sri Lanka Institute of Information Technology, Malabe 10115, Sri Lanka*

Nisal Rajapaksha − *Department of Applied Sciences, Faculty of Humanities and Sciences, Sri Lanka Institute of Information Technology, Malabe 10115, Sri Lanka*

Supuni Wijayawardana − *Department of Applied Sciences, Faculty of Humanities and Sciences, Sri Lanka Institute of Information Technology, Malabe 10115, Sri Lanka*

Udani Senevirathne − *Department of Applied Sciences, Faculty of Humanities and Sciences, Sri Lanka Institute of Information Technology, Malabe 10115, Sri Lanka*

Madara Jayanetti − *Department of Applied Sciences, Faculty of Humanities and Sciences, Sri Lanka Institute of Information Technology, Malabe 10115, Sri Lanka*

Upeka Samarakoon − *Department of Nano Science Technology, Faculty of Technology, Wayamba University of Sri Lanka, Kuliyapitiya 60416, Sri Lanka*

Complete contact information is available at: https://pubs.acs.org/10.1021/acsomega.5c08001

Funding

Sri Lanka Institute of Information Technology funded this research project.

Notes

The authors declare no competing financial interest.

■ ACKNOWLEDGMENTS

The authors acknowledge the R&D Centre, Link Natural Products (Pvt) Ltd., the University of Moratuwa, and the Sri Lanka Institute of Nanotechnology for providing instrument facilities.

■ REFERENCES

(1) Valero-Mendoza, A. G.; et al. The whole pomegranate (Punica granatum. L), biological properties and important findings: A review. *Food Chem. Adv.* **2023**, *2*, 100153.

(2) Wang, J.; Sun, M.; Yu, J.; Wang, J.; Cui, Q. Pomegranate seeds: a comprehensive review of traditional uses, chemical composition, and pharmacological properties. *Front. Pharmacol.* **2024**, *15*, 1401826.

(3) Viladomiu, M.; Hontecillas, R.; Lu, P.; Bassaganya-Riera, J. Preventive and Prophylactic Mechanisms of Action of Pomegranate Bioactive Constituents. *Evidence-Based Complement. Altern. Med.* **2013**, *2013*, 789764.

(4) Minutolo, A.; et al. Antioxidant Phytocomplexes Extracted from Pomegranate (Punica granatum L.) Using Hydrodynamic Cavitation Show Potential Anticancer Activity In Vitro. *Antioxidants* **2023**, *12*, 1560.

(5) Fathi, F.; Ebrahimi, S. N.; Pereira, D. M.; Estevinho, B. N.; Rocha, F. Preliminary studies of microencapsulation and anticancer activity of polyphenols extract from Punica granatum peels. *Can. J. Chem. Eng.* **2022**, *100*, 3240−3252.

(6) González-González, G. M.; et al. Anticancer activity of polyphenolic Punica granatum peel extracts obtained by hybrid ultrasound-microwave assisted extraction: Evaluation on HeLa and HepG2 cells. *Environ. Qual Manag* **2024**, *33*, 295−304.

(7) Hashem, A. H.; et al. Pomegranate Peel Extract Stabilized Selenium Nanoparticles Synthesis: Promising Antimicrobial Potential, Antioxidant Activity, Biocompatibility, and Hemocompatibility. *Appl. Biochem. Biotechnol.* **2023**, *195*, 5753−5776.

(8) Selahvarzi, A.; et al. Optimization of ultrasonic-assisted extraction of phenolic compounds from pomegranate and orange peels and their antioxidant activity in a functional drink. *Food Biosci.* **2022**, *49*, 101918.

(9) Esposto, S.; et al. Chemical composition, antioxidant activity, and sensory characterization of commercial pomegranate juices. *Antioxidants* **2021**, *10*, 1381.

(10) Pierdomenico, M.; Riccioni, C.; Benassi, B. Anti-inflammatory effect of a pomegranate extract on LPS-stimulated HepG2 cells. *Nat. Prod. Res.* **2024**, *38*, 727−734.

(11) Sayed, S.; et al. The Anti-Inflammatory, Anti-Apoptotic, and Antioxidant Effects of a Pomegranate-Peel Extract against Acrylamide-Induced Hepatotoxicity in Rats. *Life* **2022**, *12*, 224.

(12) Okumuş, E.; Bakkalbaşı, E. Determination of the bioaccessibility and antidiabetic properties of pomegranate peels. *J. Food Meas. Charact* **2021**, *15*, 3357−3366.

(13) Eid, A. M.; Issa, L.; Arar, K.; Abu-Zant, A.; Makhloof, M.; Masarweh, Y.; et al. Phytochemical screening, antioxidant, anti-diabetic, and anti-obesity activities, formulation, and characterization of a self-nanoemulsion system loaded with pomegranate (Punica granatum) seed oil. *Sci. Rep.* **2024**, *14* (1), 18841.

(14) Gosset-Erard, C.; Zhao, M.; Lordel-Madeleine, S.; Ennahar, S. Identification of punicalagin as the bioactive compound behind the antimicrobial activity of pomegranate (Punica granatum L.) peels. *Food Chem.* **2021**, *352*, 129396.

(15) Magangana, T. P.; et al. Blanching pre-treatment promotes high yields, bioactive compounds, antioxidants, enzyme inactivation and antibacterial activity of 'wonderful' pomegranate peel extracts at three different harvest maturities. *Antioxidants* **2021**, *10*, 1119.

(16) Haghighian, M. K.; Rafraf, M.; Hemmati, S.; Haghravan, S.; Asghari-Jafarabadi, M. Effects of pomegranate (Punica granatum L.) peel extract supplementation on serum lipid profile and oxidative stress in obese women with knee osteoarthritis: A double blind, randomized, placebo controlled study. *Adv. Integr. Med.* **2021**, *8*, 107−113.

(17) Ko, K.; Dadmohammadi, Y.; Abbaspourrad, A. Nutritional and Bioactive Components of Pomegranate Waste Used in Food and Cosmetic Applications: A Review. *Foods* **2021**, *10*, 657.

(18) Sun, Y. Q.; Tao, X.; Men, X. M.; Xu, Z. W.; Wang, T. In vitro and in vivo antioxidant activities of three major polyphenolic compounds in pomegranate peel: Ellagic acid, punicalin, and punicalagin. *J. Integr. Agric.* **2017**, *16*, 1808−1818.
(19) Vora, A.; Londhe, V.; Pandita, N. Herbosomes enhance the in vivo antioxidant activity and bioavailability of punicalagins from standardized pomegranate extract. *J. Funct. Foods* **2015**, *12*, 540−548.
(20) Samineni, R.; Chimakurthy, J.; Konidala, S. Emerging Role of Biopharmaceutical Classification and Biopharmaceutical Drug Disposition System in Dosage form Development: A Systematic Review. *Turkish J. Pharm. Sci.* **2022**, *19*, 706.
(21) Truzzi, F.; Tibaldi, C.; Zhang, Y.; Dinelli, G.; D'amen, E. An Overview on Dietary Polyphenols and Their Biopharmaceutical Classification System (BCS). *Int. J. Mol. Sci.* **2021**, *22* (11), 5514.
(22) Chen, P.; Zou, F.; Liu, W. Recent advancement in prevention against hepatotoxicity, molecular mechanisms, and bioavailability of gallic acid, a natural phenolic compound: challenges and perspectives. *Front. Pharmacol.* **2025**, *16*, 1549526.
(23) Harwansh, R. K.; Deshmukh, R.; Shukla, V. P.; Khunt, D.; Prajapati, B. G.; Rashid, S.; Ali, N.; Elossaily, G. M.; Suryawanshi, V. K.; Kumar, A.; et al. Recent Advancements in Gallic Acid-Based Drug Delivery: Applications, Clinical Trials, and Future Directions. *Pharmaceutics* **2024**, *16* (9), 1202.
(24) Mertens-Talcott, S. U.; Jilma-Stohlawetz, P.; Rios, J.; Hingorani, L.; Derendorf, H. A. Metabolism, and Antioxidant Effects of Pomegranate (Punica granatum L.) Polyphenols after Ingestion of a Standardized Extract in Healthy Human Volunteers. *J. Agric. Food Chem.* **2006**, *54*, 8956−8961.
(25) Cerdá, B.; Llorach, R.; Cerón, J. J.; Espín, J. C.; Tomás-Barberán, F. A. Evaluation of the bioavailability and metabolism in the rat of punicalagin, an antioxidant polyphenol from pomegranate juice. *Eur. J. Nutr.* **2003**, *42*, 18−28.
(26) Nyamba, I.; Lechanteur, A.; Semdé, R.; Evrard, B. Physical formulation approaches for improving aqueous solubility and bioavailability of ellagic acid: A review. *Eur. J. Pharm. Biopharm.* **2021**, *159*, 198−210.
(27) Zuccari, G.; et al. Formulation Strategies to Improve Oral Bioavailability of Ellagic Acid. *Appl. Sci.* **2020**, *10*, 3353.
(28) Mohsen, S.; Bakr, M. M.; ElDegwy, M. A.; Abouhussein, D. M. N.; Fares, A. R.; ElMeshad, A. N.; et al. Pomegranate extract-loaded surfactant-free zein nanoparticles as a promising green approach for hepatic cancer: optimization and in vitro cytotoxicity. *Futur J. Pharm. Sci.* **2024**, *10* (101), 73.
(29) Singh, M.; Lee, K. E.; Vinayagam, R.; Kang, S. G. Antioxidant and Antibacterial Profiling of Pomegranate-pericarp Extract Functionalized-zinc Oxide Nanocomposite. *Biotechnol. Bioprocess Eng.* **2021**, *26*, 728−737.
(30) Tabar, M. N.; Nateghi, L.; Ravan, M. H.; Rashidi, L. Encapsulation of walnut husk and pomegranate peel extracts by alginate and chitosan-coated nanoemulsions. *Int. J. Biol. Macromol.* **2025**, *301*, 140349.
(31) Sanhueza, L.; et al. Encapsulation of Pomegranate Peel Extract (Punica granatum L.) by Double Emulsions: Effect of the Encapsulation Method and Oil Phase. *Foods* **2022**, *11*, 310.
(32) Teaima, M. H.; et al. Efficacy of pomegranate extract loaded solid lipid nanoparticles transdermal emulgel against Ehrlich ascites carcinoma. *Nanomedicine Nanotechnology, Biol. Med.* **2022**, *39*, 102466.
(33) Ju, J.; Kim, S. D.; Shin, M. Pomegranate Polyphenol-Derived Injectable Therapeutic Hydrogels to Enhance Neuronal Regeneration. *Mol. Pharmaceutics* **2023**, *20*, 4786−4795.
(34) Soltanzadeh, M.; Peighambardoust, S. H.; Ghanbarzadeh, B.; Mohammadi, M.; Lorenzo, J. M. Chitosan Nanoparticles as a Promising Nanomaterial for Encapsulation of Pomegranate (Punica granatum L.) Peel Extract as a Natural Source of Antioxidants. *Nanomater* **2021**, *11*, 1439.
(35) Patil, P.; Killedar, S. Improving gallic acid and quercetin bioavailability by polymeric nanoparticle formulation. *Drug Dev. Ind. Pharm* **2021**, *47*, 1656−1663.
(36) Fattahi Nafchi, R.; et al. In Vitro Study: Synthesis and Evaluation of Fe3O4/CQD Magnetic/Fluorescent Nanocomposites for Targeted Drug Delivery, MRI, and Cancer Cell Labeling Applications. *Langmuir* **2022**, *38*, 3804−3816.
(37) Nordin, A. H.; et al. The State of the Art of Natural Polymer Functionalized Fe3O4Magnetic Nanoparticle Composites for Drug Delivery Applications: A Review. *Gels* **2023**, *9*, 121.
(38) Shen, L.; Li, B.; Qiao, Y. Fe3O4 Nanoparticles in Targeted Drug/Gene Delivery Systems. *Mater* **2018**, *11*, 324.
(39) Monaco, I.; et al. Synthesis of Lipophilic Core-Shell Fe3O4@SiO2@Au Nanoparticles and Polymeric Entrapment into Nanomicelles: A Novel Nanosystem for in Vivo Active Targeting and Magnetic Resonance-Photoacoustic Dual Imaging. *Bioconjugate Chem* **2017**, *28*, 1382−1390.
(40) Pramanik, A.; et al. Fluorescent, Magnetic Multifunctional Carbon Dots for Selective Separation, Identification, and Eradication of Drug-Resistant Superbugs. *ACS Omega* **2017**, *2*, 554−562.
(41) Cui, X.; et al. Sonochemical fabrication of folic acid functionalized multistimuli-responsive magnetic graphene oxide-based nanocapsules for targeted drug delivery. *Chem. Eng. J* **2017**, *326*, 839−848.
(42) Kamalzare, M.; Ahghari, M. R.; Bayat, M.; Maleki, A. Fe3O4@chitosan-tannic acid bionanocomposite as a novel nanocatalyst for the synthesis of pyranopyrazoles. *Sci. Rep.* **2021**, *11*, 20021.
(43) Liu, Z.; Wang, K.; Peng, X.; Zhang, L. Chitosan-based drug delivery systems: Current strategic design and potential application in human hard tissue repair. *Eur. Polym. J.* **2022**, *166*, 110979.
(44) Bakhshi, V.; Poursadegh, H.; Amini-Fazl, M. S.; Salari, D.; Javanbakht, S. Synthesis and characterization of bio-nanocomposite hydrogel beads based on magnetic hydroxyapatite and chitosan: a pH-sensitive drug delivery system for potential implantable anticancer platform. *Polym. Bull* **2024**, *81*, 7499−7518.
(45) Akinyelu, J.; Oladimeji, O.; Daniels, A.; Singh, M. Folate-targeted doxorubicin delivery to breast and cervical cancer cells using a chitosan-gold nano-delivery system. *J. Drug Delivery Sci. Technol.* **2022**, *67*, 102978.
(46) Norouzi, Z.; Abdouss, M. Electrospun nanofibers using β-cyclodextrin grafted chitosan macromolecules loaded with indomethacin as an innovative drug delivery system. *Int. J. Biol. Macromol.* **2023**, *233*, 123518.
(47) Zhang, S.; et al. Carboxymethyl chitosan microspheres loaded hyaluronic acid/gelatin hydrogels for controlled drug delivery and the treatment of inflammatory bowel disease. *Int. J. Biol. Macromol.* **2021**, *167*, 1598−1612.
(48) Affes, S.; et al. Chitosan derivatives-based films as pH-sensitive drug delivery systems with enhanced antioxidant and antibacterial properties. *Int. J. Biol. Macromol.* **2021**, *182*, 730−742.
(49) Shikuku, R.; et al. Chitosan-based pH-sensitive semi-interpenetrating network nanoparticles as a sustained release matrix for anticancer drug delivery. *Carbohydr. Polym. Technol. Appl.* **2024**, *7*, 100515.
(50) Aibani, N.; Rai, R.; Patel, P.; Cuddihy, G.; Wasan, E. K. Chitosan Nanoparticles at the Biological Interface. *Implications For Drug Delivery* **2021**, *13*, 1686.
(51) Luong, H. V. T.; et al. Alginate−functionalized Fe3O4 nanoparticles as a drug delivery system for targeted controlled release. *J. Drug Delivery Sci. Technol.* **2024**, *93*, 105465.
(52) Nguyen, N. Y.; Luong, H. V. T.; Pham, D. T.; Tran, T. B. Q.; Dang, H. G. Chitosan-functionalized Fe3O4@SiO2 nanoparticles as a potential drug delivery system. *Chem. Pap.* **2022**, *76*, 4561−4570.
(53) Ehteshamzadeh, T.; Kakaei, S.; Ghaffari, M.; Khanchi, A. R. Doxorubicin Embedded Polyvinylpyrrolidone-Coated Fe3O4 Nanoparticles for Targeted Drug Delivery System. *J. Supercond. Nov. Magn.* **2021**, *34*, 3345−3360.
(54) Asgari, S.; et al. Chitosan-Grafted-Poly(N-vinylcaprolactam)-Decorated Fe3O4@SiO2 Core-Shell Nanoformulation as an Efficient Drug Delivery System for Poorly Soluble Drugs. *ACS Appl. Bio Mater.* **2023**, *6*, 5809−5827.

https://doi.org/10.1021/acsomega.5c08001
ACS Omega 2025, 10, 50488−50510

(55) Patil, P.; Killedar, S. Green Approach Towards Synthesis and Characterization of GMO/Chitosan Nanoparticles for In Vitro Release of Quercetin: Isolated from Peels of Pomegranate Fruit. *J. Pharm. Innov.* **2022**, *17*, 764−777.
(56) Ebrahimnia, M.; Rabbani, S.; Mahboubi, A.; Kamalinejad, M.; Haeri, A. Preparation, antioxidant, antibacterial, and in vivo evaluation of pomegranate flower extract nanofibers based on thiolated chitosan and thiolated gelatin for treating aphthous stomatitis. *Carbohydr. Polym.* **2025**, *351*, 122971.
(57) Abuelmakarem, H. S.; et al. Investigating the Application of Pomegranate-Loaded Chitosan Nanoparticles as Contrast Agents for Enhancing Breast Cancer Detection via Diffuse Reflectance Spectroscopy. *Chemosensors* **2025**, *13*, 73.
(58) Taherian, A.; Esfandiari, N.; Rouhani, S. Breast cancer drug delivery by novel drug-loaded chitosan-coated magnetic nanoparticles. *Cancer Nanotechnol.* **2021**, *12*, 15.
(59) Zhou, G.; You, Y.; Wang, B.; Wang, S.; Liu, J. Green synthesis of magnetic Fe3O4/Ag nanocomposite using Pomegranate peel extract for the treatment of ovarian cancer. *Arab. J. Chem.* **2024**, *17*, 105394.
(60) Rashidzadeh, B.; et al. Preparation and characterization of antibacterial magnetic-/pH-sensitive alginate/Ag/Fe3O4 hydrogel beads for controlled drug release. *Int. J. Biol. Macromol.* **2020**, *154*, 134−141.
(61) Ayyanaar, S.; Kesavan, M. P. Magnetic iron oxide nanoparticles@lecithin/poly (l-lactic acid) microspheres for targeted drug release in cancer therapy. *Int. J. Biol. Macromol.* **2023**, *253*, 127480.
(62) Appu, M.; Lian, Z.; Zhao, D.; Huang, J. Biosynthesis of chitosan-coated iron oxide (Fe3O4) hybrid nanocomposites from leaf extracts of Brassica oleracea L. and study on their antibacterial potentials. *3 Biotech* **2021**, *11*, 271.
(63) Fadhel, F. S.; Nouri, S. M. Enhanced Antibacterial Activity of Artemisia vulgaris Ethanol Extract Using Chitosan-Coated Iron Oxide Nanoparticles Against Staphylococcus aureus and Klebsiella pneumoniae. *Cent. Asian J. Med. Nat. Sci.* **2025**, *6*, 2044−2055.
(64) Mphahlele, R. R.; Fawole, O. A.; Makunga, N. P.; Opara, U. L. Effect of drying on the bioactive compounds, antioxidant, antibacterial and antityrosinase activities of pomegranate peel. *BMC Complement Altern. Med.* **2016**, *16*, 143.
(65) Ba-Abbad, M. M.; Benamour, A.; Ewis, D.; Mohammad, A. W.; Mahmoudi, E. Synthesis of Fe3O4 Nanoparticles with Different Shapes Through a Co-Precipitation Method and Their Application. *JOM* **2022**, *74*, 3531−3539.
(66) Mendis, A.; Thambiliyagodage, C.; Ekanayake, G.; Liyanaarachchi, H.; Jayanetti, M.; Vigneswaran, S.; et al. Fabrication of Naturally Derived Chitosan and Ilmenite Sand-Based TiO2/Fe2O3/Fe-N-Doped Graphitic Carbon Composite for Photocatalytic Degradation of Methylene Blue under Sunlight. *Molecules* **2023**, *28* (7), 3154.
(67) Toledo-Merma, P. R.; et al. Phenolic Compounds Recovery from Pomegranate (Punica granatum L.) By-Products of Pressurized Liquid Extraction. *Foods* **2022**, *11*, 1070.
(68) Wijayawardana, S.; Thambiliyagodage, C.; Jayanetti, M. Kinetic study of in vitro release of curcumin from chitosan biopolymer and the evaluation of biological efficacy. *Arab. J. Chem.* **2024**, *17*, 105896.
(69) Ketsuwan, N.; Leelarungrayub, J.; Kothan, S.; Singhatong, S. Antioxidant compounds and activities of the stem, flower, and leaf extracts of the anti-smoking Thai medicinal plant: Vernonia cinerea Less. *Drug Des. Devel. Ther.* **2017**, *11*, 383−391.
(70) Viswanadha, L. S.; Arcot, Y.; Lin, Y. T.; Akbulut, M. E. S. A comparative investigation of release kinetics of paclitaxel from natural protein and macromolecular nanocarriers in nanoscale drug delivery systems. *JCIS Open* **2024**, *15*, 100120.
(71) Romeo, F. V.; et al. Chemical Characterization of Different Sumac and Pomegranate Extracts Effective against Botrytis cinerea Rots. *Molecules* **2015**, *20*, 11941.
(72) Haghighi, Y. V.; Sabahi, H.; Salamat, S. Assessment of the Influence of Saffron Pollen and Saffron Pollen/Rutin Microcapsules on Thermal and Oxidative Stability of Edible Oil: Thermogravimetric Study. *ACS Food Sci. Technol* **2023**, *3*, 1014−1020.
(73) Jafari, Y.; Sabahi, H.; Rezayan, A. H. Stability and loading properties of Curcumin encapsulated in saffron pollen. *Food Chem. Adv.* **2025**, *7*, 101009.
(74) García, P.; et al. Recovery of Bioactive Compounds from Pomegranate (Punica granatum L.) Peel Using Pressurized Liquid Extraction. *Foods* **2021**, *10*, 203.
(75) Muñiz-Márquez, D. B.; et al. Effect of ultrasound on the extraction of ellagic acid and hydrolysis of ellagitannins from pomegranate husk. *Environ. Technol. Innov.* **2021**, *24*, 102063.
(76) Parisi, V.; et al. Comparative Chemical Analysis of Eight Punica granatum L. Peel Cultivars and Their Antioxidant and Anti-Inflammatory Activities. *Antioxidants* **2022**, *11*, 2262.
(77) Lee, C. J.; Chen, L. G.; Liang, W. L.; Hsieh, M. S.; Wang, C. C. Inhibitory effects of punicalagin from Punica granatum against type II collagenase-induced osteoarthritis. *J. Funct. Foods* **2018**, *41*, 216−222.
(78) Fawole, O. A.; Makunga, N. P.; Opara, U. L. Antibacterial, antioxidant and tyrosinase-inhibition activities of pomegranate fruit peel methanolic extract. *BMC Complement Altern. Med.* **2012**, *12*, 200.
(79) Benchagra, L.; et al. Antioxidant effect of moroccan pomegranate (Punica granatum L. sefri variety) extracts rich in punicalagin against the oxidative stress process. *Foods* **2021**, *10*, 2219.
(80) Taha Yassin, M.; Mostafa, A. A.-F.; Al Askar, A. A.; et al. In Vitro Evaluation of Biological Activities and Phytochemical Analysis of Different Solvent Extracts of Punica granatum L. (Pomegranate) Peels. *Plants* **2021**, *10* (12), 2742.
(81) Dogara, A. M.; Hama, H. A.; Ozdemir, D. Update on the Potential of Punica granatum L. Traditional Uses and Pharmacological Uses: A Review. *Adv. Pharmacol. Pharm. Sci.* **2024**, *2024* (1), 6523809.
(82) Aruna, P.; Venkataramanamma, D.; Singh, A. K.; Singh, R. P. Health Benefits of Punicic Acid: A Review. *Compr. Rev. Food Sci. Food Saf.* **2016**, *15*, 16−27.
(83) Kandylis, P.; Kokkinomagoulos, E. Food Applications and Potential Health Benefits of Pomegranate and its Derivatives. *Foods* **2020**, *9*, 122.
(84) Kohno, H.; et al. Pomegranate seed oil rich in conjugated linolenic acid suppresses chemically induced colon carcinogenesis in rats. *Cancer Sci.* **2004**, *95*, 481−486.
(85) Tehranifar, A.; Selahvarzi, Y.; Kharrazi, M.; Bakhsh, V. J. High potential of agro-industrial by-products of pomegranate (Punica granatum L.) as the powerful antifungal and antioxidant substances. *Ind. Crops Prod.* **2011**, *34*, 1523−1527.
(86) Soleymanfallah, S.; Khoshkhoo, Z.; Hosseini, S. E.; Azizi, M. H. Preparation, physical properties, and evaluation of antioxidant capacity of aqueous grape extract loaded in chitosan-TPP nanoparticles. *Food Sci. Nutr.* **2022**, *10*, 3272−3281.
(87) Wan, A.; Xu, Q.; Sun, Y.; Li, H. Antioxidant activity of high molecular weight chitosan and N,O-quaternized chitosans. *J. Agric. Food Chem.* **2013**, *61*, 6921−6928.
(88) Tomida, H.; et al. Antioxidant properties of some different molecular weight chitosans. *Carbohydr. Res.* **2009**, *344*, 1690−1696.
(89) Hromis, N.; Lazic, V.; Popovic, S.; Suput, D.; Bulut, S. Antioxidative activity of chitosan and chitosan based biopolymer film. *Food Feed Res.* **2017**, *44*, 91−100.
(90) Alsharabasy, A. Semi-synthesis of Chitosan with High Molecular Weight and Enhanced Deacetylation Degree Amir. *Polym. Sci.* **2016**, *2*, 11.
(91) Ullah, M.; Kim, D. S.; Hun Park, K. Evaluating antioxidant activity of phenolic mediated Fe3O4 nanoparticles using Usnea Longissimma methanol extract. *Results Chem.* **2022**, *4*, 100661.
(92) Patra, J. K.; Ali, M. S.; Oh, I. G.; Baek, K. H. Proteasome inhibitory, antioxidant, and synergistic antibacterial and anticandidal activity of green biosynthesized magnetic Fe3O4 nanoparticles using the aqueous extract of corn (Zea mays L.) ear leaves. *Artif. Cells, Nanomed., Biotechnol.* **2017**, *45*, 349−356.
(93) Alshehri, M. A.; Panneerselvam, C. Development of quercetin loaded biosynthesized chitosan grafted iron oxide nanoformulation

https://doi.org/10.1021/acsomega.5c08001
ACS Omega 2025, 10, 50488−50510

and their antioxidant, antibacterial, and anti-cancer properties. *J. Drug Delivery Sci. Technol.* **2024**, *101*, 106247.
(94) Anokwah, D.; Kwatia, E.A.; Amponsah, I.K.; Jibira, Y.; Harley, B.K.; Ameyaw, E.O.; Obese, E.; Biney, R.P.; Mensah, A.Y. Evaluation of the anti-inflammatory and antioxidant potential of the stem bark extract and some constituents of Aidia genipiflora (DC.) dandy (rubiaceae). *Heliyon* **2022**, *8*, No. e10082.
(95) Khatun, M.; Nur, M. A.; Biswas, S.; Khan, M.; Amin, M. Z. Assessment of the anti-oxidant, anti-inflammatory and anti-bacterial activities of different types of turmeric (Curcuma longa) powder in Bangladesh. *J. Agric. Food Res.* **2021**, *6*, 100201.
(96) Saeed, E.; Javed, F.; Rana, Z.; Perveen, R.; Mallhi, I. Y.; Amjad, I.; Maqsood, Q.; Chaudhary, N. A.; Tahir, S. B.; Fatima, A.; et al. Bioactive Compounds, Their Mechanisms of Action, and Cardioprotective Effects of Pomegranate (Punica granatum): A Comprehensive Review. *eFood* **2025**, *6* (4), No. e70075.
(97) Cordiano, R.; Gammeri, L.; Di Salvo, E.; Gangemi, S.; Minciullo, P. L. Pomegranate (Punica granatum L.) Extract Effects on Inflammaging. *Mol* **2024**, *29*, 4174.
(98) Jafarirad, S.; Goodarzi, R.; Mohammadtaghvaei, N.; Dastoorpoor, M.; Alavinejad, P. Effectiveness of the pomegranate extract in improving hepatokines and serum biomarkers of non-alcoholic fatty liver disease: A randomized double blind clinical trial. *Diabetes Metab. Syndr. Clin. Res. Rev.* **2023**, *17*, 102693.
(99) Ruan, J.; et al. Novel oral administrated ellagic acid nanoparticles for enhancing oral bioavailability and anti-inflammatory efficacy. *J. Drug Delivery Sci. Technol.* **2018**, *46*, 215−222.
(100) Saafane, A.; Girard, D. Interaction between iron oxide nanoparticles (Fe3O4 NPs) and human neutrophils: Evidence that Fe3O4 NPs possess some pro-inflammatory activities. *Chem. Biol. Interact* **2022**, *365*, 110053.
(101) Bheemayya, L.; Kamble, R.; Shettar, A.; Nadoni, V.; Nayak, M.; Joshi, S.; Bayannavar, P.; Metre, T.; Keri, R.; Hoskeri, J.; et al. Microwave-Assisted Fe3O4 Nanoparticles Catalyzed Cascade Synthesis of 3-(1,4,5-Triaryl-1H-imidazol-2yl)quinolin-2-amines as COX-1, COX-2 Inhibitors and Antioxidant Agents. *Appl. Organomet. Chem.* **2025**, *39* (2), No. e7812.
(102) Mohyuddin, S. G.; Qamar, A.; Hu, C.Y.; Chen, S.W.; Wen, J.Y.; Liu, X.X.; Ma, X.B.; Yu, Z.C.; Yong, Y.H.; Wu, L.Y.; et al. Effect of chitosan on blood profile, inflammatory cytokines by activating TLR4/NF-κB signaling pathway in intestine of heat stressed mice. *Sci. Rep.* **2021**, *11*, 20608.
(103) Tian, Y.; Xu, Z.; Zheng, B.; Martin Lo, Y. Optimization of ultrasonic-assisted extraction of pomegranate (Punica granatum L.) seed oil. *Ultrason. Sonochem* **2013**, *20*, 202−208.
(104) Goula, A. M.; Adamopoulos, K. G. A method for pomegranate seed application in food industries: Seed oil encapsulation. *Food Bioprod. Process* **2012**, *90*, 639−652.
(105) Singh, B.; Singh, J. P.; Kaur, A.; Singh, N. Phenolic compounds as beneficial phytochemicals in pomegranate (Punica granatum L.) peel: A review. *Food Chem.* **2018**, *261*, 75−86.
(106) Saparbekova, A. A.; Kantureyeva, G. O.; Kudasova, D. E.; Konarbayeva, Z. K.; Latif, A. S. Potential of phenolic compounds from pomegranate (Punica granatum L.) by-product with significant antioxidant and therapeutic effects: A narrative review. *Saudi J. Biol. Sci.* **2023**, *30*, 103553.
(107) Elendran, S.; Shiva Kumar, V.; Sundralingam, U.; Tow, W. K.; Palanisamy, U. D. Enhancing the Bioavailability of the Ellagitannin, Geraniin: Formulation, Characterization, and in vivo Evaluation. *Int. J. Pharm.* **2024**, *660*, 124333.
(108) El-Missiry, M. A.; et al. Nanoformulated ellagic acid ameliorates pentylenetetrazol-induced experimental epileptic seizures by modulating oxidative stress, inflammatory cytokines and apoptosis in the brains of male mice. *Metab. Brain Dis.* **2020**, *35*, 385−399.
(109) Abd-Rabou, A. A.; Ahmed, H. H. CS-PEG decorated PLGA nano-prototype for delivery of bioactive compounds: A novel approach for induction of apoptosis in HepG2 cell line. *Adv. Med. Sci.* **2017**, *62*, 357−367.
(110) Jebahi, S.; et al. Chitosan-Based Gastric Dressing Materials Loaded with Pomegranate Peel as Bioactive Agents: Pharmacokinetics and Effects on Experimentally Induced Gastric Ulcers in Rabbits. *Metab* **2022**, *12*, 1158.
(111) Badawi, N. M.; et al. Pomegranate extract-loaded solid lipid nanoparticles: Design, optimization, and in vitro cytotoxicity study. *Int. J. Nanomed.* **2018**, *13*, 1313−1326.
(112) Anwer, M. K.; Alshdefat, R.; Akhtar, J.; Aleemuddin, M. Punica granatum Loaded Glycerosomes for Antibacterial Effect in Skin Infections: Preparation, Optimization, In Vitro and In Vivo Characterization. *BioNanosci* **2025**, *15* (2), 294.
(113) El-Hamid, M. I. A.; Ibrahim, D.; Abdelfattah-Hassan, A.; Mohammed, O. B.; Pet, I.; Khalil, S. S.; El-Badry, S. M.; Metwally, A. S.; Azouz, A. A.; Elnegiry, A. A.; et al. Silver nanoparticles loaded with pomegranate peel extract and hyaluronic acid mediate recovery of cutaneous wounds infected with Candida albicans. *Front. Cell. Infect. Microbiol.* **2024**, *14*, 1469493.
(114) Al-Qarhami, F.; Abdallah, A. B.; Khalifa, M. E.; Awad, F. S. Glutaraldehyde-crosslinked magnetic chitosan nanocomposite for efficient Cr(VI) removal: A sustainable approach to aquatic remediation. *Int. J. Biol. Macromol.* **2025**, *310*, 143459.
(115) Pavoni, J. M. F.; dos Santos, N. Z.; May, I. C.; Pollo, L. D.; Tessaro, I. C. Impact of acid type and glutaraldehyde crosslinking in the physicochemical and mechanical properties and biodegradability of chitosan films. *Polym. Bull* **2021**, *78*, 981−1000.
(116) Hu, H.; Hu, H.; Xin, J. H.; Chan, A.; He, L. Glutaraldehyde-chitosan and poly (vinyl alcohol) blends, and fluorescence of their nano-silica composite films. *Carbohydr. Polym* **2013**, *91*, 305−313.
(117) Siepmann, J.; Siepmann, F. Modeling of diffusion controlled drug delivery. *J. Controlled Release* **2012**, *161*, 351−362.
(118) Khalbas, A. H.; Albayati, T. M.; Ali, N. S.; Salih, I. K. Drug loading methods and kinetic release models using of mesoporous silica nanoparticles as a drug delivery system: A review. *South African J. Chem. Eng.* **2024**, *50*, 261−280.
(119) Hillery, A. M.; Park, K.; Drug delivery: Fundamentals and applications: Second edition. *Drug Delivery Fundam. Appl. Second Ed.* CRC Press, 2016, 1−614.
(120) Kamaly, N.; Yameen, B.; Wu, J.; Farokhzad, O. C. Degradable controlled-release polymers and polymeric nanoparticles: Mechanisms of controlling drug release. *Chem. Rev.* **2016**, *116*, 2602−2663.
(121) Trucillo, P. Drug Carriers: A Review on the Most Used Mathematical Models for Drug Release. *Processes* **2022**, *10* (6), 1094.
(122) Unagolla, J. M.; Jayasuriya, A. C. Drug transport mechanisms and in vitro release kinetics of vancomycin encapsulated chitosan-alginate polyelectrolyte microparticles as a controlled drug delivery system. *Eur. J. Pharm. Sci.* **2018**, *114*, 199−209.
(123) İlgar, M.; Karakuş, S.; Kilislioğlu, A. Design, characterization and evaluation of the drug-loaded chitosan/cerium oxide nanoparticles with pH-controlled drug release. *Polym. Bull* **2022**, *79*, 6693−6708.
(124) Amini-Fazl, M. S.; Mobedi, H. Investigation of mathematical models based on diffusion control release for Paclitaxel from in-situ forming PLGA microspheres containing HSA microparticles. *Mater. Technol.* **2020**, *35*, 50−59.
(125) Eldeeb, A. M.; Serag, E.; Elmowafy, M.; El-Khouly, M. E. pH-responsive zeolite-A/chitosan nanocarrier for enhanced ibuprofen drug delivery in gastrointestinal systems. *Int. J. Biol. Macromol.* **2025**, *289*, 138879.
(126) Rashidi, Z.; Bagheri Marandi, G.; Taghvay Nakhjiri, M. Carboxymethyl cellulose-based nanocomposite hydrogel grafted with vinylic comonomers: synthesis, swelling behavior and drug delivery investigation. *J. Macromol. Sci., Part A: pure Appl. Chem.* **2022**, *59*, 421−432.
(127) Özkahraman, B.; Acar, I.; Güçlü, G. Synthesis of N-vinylcaprolactam and methacrylic acid based hydrogels and investigation of drug release characteristics. *Polym. Bull* **2023**, *80*, 5149−5181.

https://doi.org/10.1021/acsomega.5c08001
ACS Omega 2025, 10, 50488−50510

(128) Jayachandran, P.; et al. Green Synthesized Silver Nanoparticle-Loaded Liposome-Based Nanoarchitectonics for Cancer Management: In Vitro Drug Release Analysis. *Biomed* **2023**, *11*, 217.
(129) Khan, M. U. A.; et al. Chitosan/Poly Vinyl Alcohol/Graphene Oxide Based pH-Responsive Composite Hydrogel Films: Drug Release, Anti-Microbial and Cell Viability Studies. *Polymer* **2021**, *13*, 3124.
(130) Rajabzadeh-Khosroshahi, M.; et al. Chitosan/agarose/graphitic carbon nitride nanocomposite as an efficient pH-sensitive drug delivery system for anticancer curcumin releasing. *J. Drug Delivery Sci. Technol.* **2022**, *74*, 103443.
(131) Uhljar, L. É.; et al. In Vitro Drug Release, Permeability, and Structural Test of Ciprofloxacin-Loaded Nanofibers. *Pharm* **2021**, *13*, 556.
(132) Zauška, Ľ.; et al. Adsorption and Release Properties of Drug Delivery System Naproxen-SBA-15: Effect of Surface Polarity, Sodium/Acid Drug Form and pH. *J. Funct. Biomater.* **2022**, *13*, 275.
(133) Tambe, S.; Jain, D.; Amin, P. Simultaneous determination of dorzolamide and timolol by first-order derivative UV spectroscopy in simulated biological fluid for in vitro drug release testing. *Spectrochim. Acta, Part A* **2021**, *255*, 119682.
(134) Wu, Y.; et al. The Fabrication of Docetaxel-Containing Emulsion for Drug Release Kinetics and Lipid Peroxidation. *Pharm* **2022**, *14*, 1993.
(135) Len, A.; et al. Physicochemical characterization and drug release properties of methyl-substituted silica xerogels made using sol−gel process. *Int. J. Mol. Sci.* **2021**, *22*, 9197.
(136) Sahu, K. M.; Biswal, A.; Manisha, U.; Swain, S. K. Synthesis and drug release kinetics of ciprofloxacin from polyacrylamide/dextran/carbon quantum dots (PAM/Dex/CQD) hydrogels. *Int. J. Biol. Macromol.* **2024**, *269*, 132132.
(137) Rasheed, R.; et al. Design of γ-alumina/chitosan/CeO2/SrO nanohydrogel for levofloxacin delivery. *Inorg. Chem. Commun.* **2025**, *178*, 114557.
(138) Soltany, P.; Miralinaghi, M.; Pajoum Shariati, F. Folic acid conjugated poly (Amidoamine) dendrimer grafted magnetic chitosan as a smart drug delivery platform for doxorubicin: In-vitro drug release and cytotoxicity studies. *Int. J. Biol. Macromol.* **2024**, *257*, 127564.
(139) Jelonek, K.; et al. Comparison of pla-based micelles and microspheres as carriers of epothilone b and rapamycin. The effect of delivery system and polymer composition on drug release and cytotoxicity against mda-mb-231 breast cancer cells. *Pharmaceutics* **2021**, *13*, 1881.
(140) Wang, Z.; Ye, Q.; Yu, S.; Akhavan, B. Poly Ethylene Glycol (PEG)-Based Hydrogels for Drug Delivery in Cancer Therapy: A Comprehensive Review. *Adv. Healthcare Mater.* **2023**, *12* (18), 2300105.
(141) Leslie, T. K.; et al. Sodium channels and the ionic microenvironment of breast tumours. *J. Physiol.* **2023**, *601*, 1543−1553.
(142) Naderi, Z.; Azizian, J. Synthesis and characterization of carboxymethyl chitosan/Fe3O4 and MnFe2O4 nanocomposites hydrogels for loading and release of curcumin. *J. Photochem. Photobiol. B Biol.* **2018**, *185*, 206−214.
(143) Márton, P.; et al. Wetting and swelling behaviour of N-acetylated thin chitosan coatings in aqueous media. *Heliyon* **2024**, *10*, No. e23201.
(144) More, P. R.; Arya, S. S. Extraction of bioactives from pomegranate peels using aqueous biphasic separation (ABPS): An optimization and bioactive profiling. *Biomass Convers. Biorefin.* **2024**, 1−15.
(145) Molski, M. Theoretical study on the radical scavenging activity of gallic acid. *Heliyon* **2023**, *9* (1), No. e12806.
(146) Ardean, C.; et al. Factors influencing the antibacterial activity of chitosan and chitosan modified by functionalization. *Int. J. Mol. Sci.* **2021**, *22*, 7449.
(147) Halake, K.; et al. Applications Using the Metal Affinity of Polyphenols with Mussel-Inspired Chemistry. *Macromol. Res.* **2018**, *26*, 93−99.
(148) Ahmadi, F.; Oveisi, Z.; Samani, M.; Amoozgar, Z. Chitosan based hydrogels: characteristics and pharmaceutical applications. *Res. Pharm. Sci.* **2015**, *10* (1), 1−16.
(149) Askarizadeh, M.; Esfandiari, N.; Honarvar, B.; Sajadian, S. A.; Azdarpour, A. Kinetic Modeling to Explain the Release of Medicine from Drug Delivery Systems. *ChemBioEng. Rev.* **2023**, *10*, 1006−1049.
(150) Jadidi, A.; Davoodian, F.; Salahinejad, E. Effect of poly lactic-co-glycolic acid encapsulation on drug delivery kinetics from vancomycin-impregnated Ca-Mg silicate scaffolds. *Prog. Org. Coat.* **2020**, *149*, 105970.
(151) Peppas, N. A.; Narasimhan, B. Mathematical models in drug delivery: How modeling has shaped the way we design new drug delivery systems. *J. Controlled Release.* **2014**, *190*, 75−81.
(152) Laracuente, M. L.; Yu, M. H.; McHugh, K. J. Zero-order drug delivery: State of the art and future prospects. *J. Controlled Release.* **2020**, *327*, 834−856.
(153) Jiang, K.; Zhou, X.; He, T. The synthesis of bacterial cellulose-chitosan zwitterionic hydrogels with pH responsiveness for drug release mechanism of the naproxen. *Int. J. Biol. Macromol.* **2022**, *209*, 814−824.
(154) Zhang, C.; et al. Oral colon-targeted mucoadhesive micelles with enzyme-responsive controlled release of curcumin for ulcerative colitis therapy. *Chin. Chem. Lett.* **2022**, *33*, 4924−4929.
(155) Zhang, Z.; et al. Encapsulation of bifidobacterium in alginate microgels improves viability and targeted gut release. *Food Hydrocoll* **2021**, *116*, 106634.
(156) Nazir, S.; et al. Nanocomposite hydrogels for melanoma skin cancer care and treatment: In-vitro drug delivery, drug release kinetics and anti-cancer activities. *Arab. J. Chem.* **2021**, *14*, 103120.
(157) Schrade, S.; Ritschl, L.; Süss, R.; Schilling, P.; Seidenstuecker, M. Gelatin Nanoparticles for Targeted Dual Drug Release out of Alginate-di-Aldehyde-Gelatin Gels. *Gels* **2022**, *8*, 365.
(158) Vajhadin, F.; Mazloum-Ardakani, M.; Raeisi, S.; Hemati, M.; Ebadi, A.; Haghiralsadat, F.; Tofighi, D.; et al. Glutaraldehyde crosslinked doxorubicin promotes drug delivery efficiency using cobalt ferrite nanoparticles. *Colloids Surf., B* **2022**, *220*, 112870.
(159) Krishnakumar, G. S.; Sampath, S.; Muthusamy, S.; John, M. A. Importance of crosslinking strategies in designing smart biomaterials for bone tissue engineering: A systematic review. *Mater. Sci. Eng., C* **2019**, *96*, 941−954.
(160) Casali, D. M.; Yost, M. J.; Matthews, M. A. Eliminating glutaraldehyde from crosslinked collagen films using supercritical CO2. *J. Biomed. Mater. Res., Part A* **2018**, *106*, 86−94.
(161) Lotfi, S.; Bahari, A.; Mahjoub, S. In vitro biological evaluations of Fe3O4 compared with core−shell structures of chitosan-coated Fe3O4 and polyacrylic acid-coated Fe3O4 nanoparticles. *Res. Chem. Intermed* **2019**, *45*, 3497−3512.
(162) Tou, P.-T.; Pelegrino, M. T.; Pieretti, J. C.; Andrade, G. P.; Cerchiaro, G.; Seabra, A. B.; et al. Synthesis, characterization and cytotoxicity of chitosan-coated Fe3O4 nanoparticles functionalized with ascorbic acid for biomedical applications. *J. Phys.: conf. Ser.* **2019**, *1323* (1), 012015.
(163) Fahmy, H. M.; Shekewy, S.; Elhusseiny, F. A.; Elmekawy, A. Enhanced Biocompatibility by Evaluating the Cytotoxic and Genotoxic Effects of Magnetic Iron Oxide Nanoparticles and Chitosan on Hepatocellular Carcinoma Cells (HCC). *Cell Biochem. Biophys.* **2024**, *82*, 1027−1042.

https://doi.org/10.1021/acsomega.5c08001
ACS Omega 2025, 10, 50488−50510